

Hotspots and Hot Moments of Metal Mobilization: Dynamic Connectivity in Legacy Mine Waters

Anita Alexandra Sanchez^{1,2*}, Maximilian P. Lau^{1,2}, Sean Adam^{1,3}, Sabrina Hedrich^{1,4}, & Conrad Jackisch^{1,3}

¹Interdisciplinary Environmental Research Centre, Technische Universität Bergakademie Freiberg, Freiberg, 09599, Germany

²Institute of Mineralogy, Technische Universität Bergakademie Freiberg, Freiberg, 09599, Germany

³Institute of Drilling Technology and Fluid Mining, Technische Universität Bergakademie Freiberg, Freiberg, 09599, Germany

⁴Institute of Biosciences, Technische Universität Bergakademie Freiberg, Freiberg, 09599, Germany

Correspondence to: Anita Alexandra Sanchez (Anita.Sanchez@mineral.tu-freiberg.de)

Abstract. Monitoring and treatment of contaminated mine water conventionally focuses on end-of-pipe assessment and remediation techniques, at the downstream outlet of mining sites after closure. Conversely, the initial stages of pollutant release and their pathways within abandoned mines have been largely overlooked. This study examines subsurface mining-affected anthropogenic structures and the dynamic hydrogeochemical loadings in terms of temporal increases in concentration and drainage pathways within them, revealing how variable subsurface flow activation impacts metal(loid) mobilization and opens novel direct mitigation options. We identified complex hydrological patterns through the mine (Reiche Zeche, Ore Mountains, Germany) in which percolation paths were dynamically connected to the drainage based on flow conditions. Using in-situ sensors, hydrogeochemical monitoring and stable water isotopes, we reveal a hydrodynamic regime in which episodic shifts in subsurface connectivity govern metal(loid) mobilization from localized storage zones, ultimately controlling solute export to surface waters. We use concentration–discharge (C–Q) relationships, the Pollution Load Index (PLI), and hydrological concepts to evaluate metal transport during the annual pattern of flow regimes. Our analyses of event-scale C–Q patterns reveal site- and element-specific shifts in flow path activation in a very short time. Low flow periods are often considered low risk for contaminant mobilization, yet contaminant hotspots within poorly connected hydrological zones can emerge during these times. The resulting high pollution potential and solute accumulation are governed by the sequence and timing of crossing or exceeding a connectivity or flow threshold, as described by fill-and-spill and lotic-lentic cycle concepts. Notably, Zn loads (in terms of flux) during low flow, pre-flush periods reached values up to six times higher than median values. Preceding the flushing events, geochemical and microbial-mediated metal leaching create the spatially distributed contaminant stock, remobilized during reconnection events. With a large proportion of heavy metal loads occurring during low flow and especially just before the high flow (flush) period, source-related, decentralized water treatment structures become much more feasible than end-of-pipe solutions that require higher throughput volumes and multi-element filtering. This work also highlights the need for event-sensitive monitoring and treatment strategy options that prioritize internal system behavior to mitigate pollution risk in abandoned mines and other cavernous hydrological systems.

32 **1 Introduction**

33 Metal mining has left a pervasive global legacy of water contamination, particularly in river basins downstream of historic and
34 active metal extraction zones (Macklin et al., 2023; Sergeant et al., 2022). Mine drainage affects more than 23 million people
35 and thousands of kilometers of rivers globally, with risks that span decades to centuries after mine closure (Macklin et al.,
36 2025). Despite regulatory progress, abandoned mine sites often lack monitoring and management, leaving communities and
37 aquatic habitats vulnerable to pollution pulses triggered by hydrological events or anthropogenic disturbances. Standard
38 monitoring under the European Water Framework Directive (WFD) and conventional water quality assessments (LAWA,
39 2003) typically rely on infrequent, low-resolution measurements providing only limited snapshots of hydrogeochemical
40 processes (Resongles et al., 2015).

41 The consequences are particularly evident in regions with long mining histories, such as the Ore Mountains of Central Europe.
42 Here, as in many former mining areas, legacy pollutants from underground workings pose environmental threats long after
43 extraction has ceased (Huang et al., 2023; Liu et al., 2014) for example in the form of diffuse and point-source runoff of acidic
44 waters bearing high concentrations of metals and sulfates (Bozau and Liessmann, 2017; Haferburg et al., 2022). While much
45 attention has focused on surface water systems downstream former mining sites, the internal hydrogeochemical dynamics of
46 underground mine workings remain poorly understood, especially in relation to episodic contaminant mobilization and non-
47 conservative transport (Hudson et al., 2018; Datta et al., 2016). Addressing these blind spots is critical for understanding
48 pollution behavior in mining-impacted systems and for designing effective remediation strategies.

49 Despite visible surface effects, the contaminant sources and pathways within abandoned underground mines remain largely
50 obscured due to limited accessibility. Seeping waters infiltrate the mining system through complex pathways along
51 underground waste rock deposits. While percolating or flowing through a fractured system of pools and pathways, waters
52 dissolve and transport various elements. This suggests that pollution is not created continuously and diffuse but instead
53 governed by discrete, intermittent and dynamically connective pathways. With hydrologic connectivity (Freeman et al., 2007)
54 and intermittency (Fovet et al., 2021) known to impose specific characteristics on water-mediated transport and turnover in
55 soil and other environments (Turnbull et al., 2018), the hydrological processes underlying contaminant mobilization and
56 dispersal in abandoned mines may be better described using the tools and concepts of fill-and-spill (McDonnell et al., 2021)
57 or lotic-lentic cycles (Schmadel et al., 2018).

58 In natural hydrologic systems, drainage connectivity, which controls water and solute transport, is shaped by catchment
59 topography and becomes activated under specific hydro-meteorological conditions such as antecedent moisture, precipitation,
60 infiltration, and subsurface flow through soil and fractured rock (Knapp et al., 2020; Li et al., 2017; Musolff et al., 2017;
61 Lemenkova et al., 2021). In mining systems, infiltration water often enters deep storage zones where percolation is retarded.
62 As a result, near-surface signals such as rainfall or snowmelt become lagged (delayed before appearing in discharge), low-pass
63 filtered (short, high-frequency variations are damped), and threshold-dependent (hydrological or geochemical responses
64 only occur once storage limits are exceeded). Given the dispersed flow paths through subsurface waste rock deposits and other

anthropogenic preferential flow paths, various fill-and-spill pools overlay. To decipher the diffuse source pattern, the closer the analysis can get to the individual sources and the higher the temporal resolution, the clearer should the mobilization pattern be revealed.

Stable water isotopes ($\delta^2\text{H}$, $\delta^{18}\text{O}$) are useful tracers for identifying flow paths, water pool mixing, and water-rock interactions (e.g., Sprenger et al., 2016; Spangenberger et al., 2007; Clark and Fritz, 2007; Kumar et al., 2024). Though widely used in ecohydrology, isotopic tools remain underutilized in mine drainage studies. We suggest that they could provide a promising means of tracing complex contaminant sources and transport processes (Ghomshei and Allen, 2000; Allen and Voormeji, 2002; Hazen et al., 2002). Similar to surface catchments, mine systems experience episodic flushing during reactivation of subsurface flow paths, when accumulated contaminants are rapidly mobilized following re-wetting periods. These short-lived first-flush events produce sharp concentration peaks before dilution or source depletion occurs (Merritt and Power, 2022; Bryne et al., 2012).

Concentration-discharge (C-Q) analysis provides a complementary approach to characterize such flow-phase-dependent behavior and have seen broad application in watersheds (Shaw et al., 2020; Rose et al., 2018; Godsey et al., 2009; Knapp et al., 2020; Musolff et al., 2015). Stable C-Q relationships indicate chemostatic conditions, often linked to proportional weathering increases (Godsey et al., 2009; Li et al., 2017) and homogeneous solute distribution (Herndon et al., 2015), whereas enrichment or dilution patterns (chemodynamic behavior) reveal heterogeneity in solute storage and mobilization (Herndon et al., 2015). However, recent work emphasizes that while C-Q tools are widely used, they are often under-contextualized and over-interpreted in isolation, and their diagnostic value depends heavily on integrating them with additional hydrological and biogeochemical information (Knapp and Musolff, 2024). Despite this, C-Q tools and associated metrics (e.g., C-Q slope, hysteresis indices, ratio of the coefficients of variation of concentration and discharge (CV_c/CV_q)) remains minimal in underground systems, where episodic connectivity complicate their interpretation, representing a methodological gap this study seeks to address.

Building on our previous study that identified strong spatial and temporal heterogeneity in contaminant release within the Reiche Zeche mine (Sanchez et al., 2025), this work investigates how dynamic hydrological and geochemical processes generate short-lived but critical contaminant release events. We focus on identifying hotspots, defined as spatial zones of disproportionately high contaminant accumulation, and hot moments, defined as short time periods when mobilization rates are markedly elevated due to transient changes in hydrological connectivity (McClain et al., 2003). The overarching research question guiding this study is: How can dynamic contaminant mobilization within underground mine systems be effectively monitored and translated into targeted, in-situ treatment strategies that move beyond conventional end-of-pipe approaches? We hypothesize that alternating hydrological flow phases control dynamic connectivity and thus metal mobilization, with C-Q patterns revealing the behavior of localized pools within the mine. To address our research question and hypothesis, our specific objectives were: (1) to characterize the temporal evolution of flow regimes and their influence on metal(lloid) concentrations and loads, (2) to determine the geochemical signatures associated with localized storage and release zones

98 (hotspots) and episodic release events (hot moments), and (3) to evaluate how phase-dependent flow and C-Q relationships
99 can inform adaptive, near-source mine water treatment strategies.

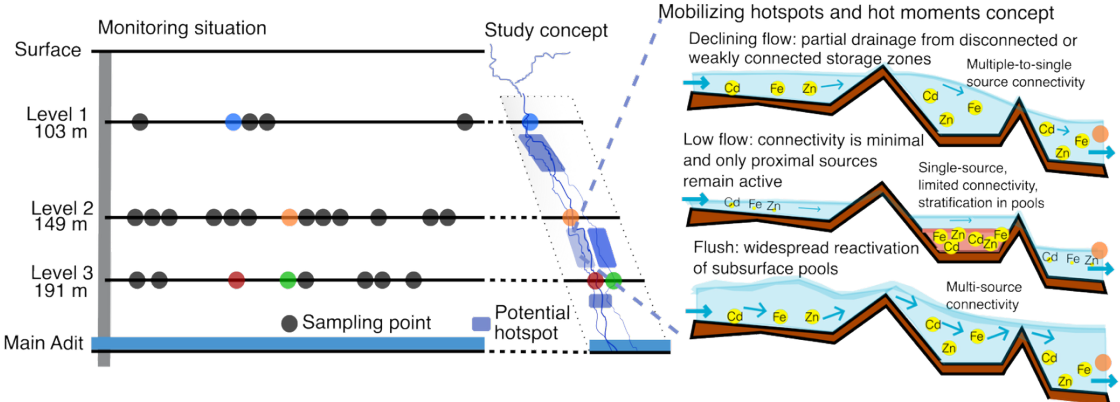
100 Therefore, we performed 42 underground sampling campaigns and utilized in-situ sensors across four distinct flow paths for
101 over two years. At one site, we conducted high-resolution and high-frequency monitoring using an in-situ UV-Vis spectrometer
102 to capture transient fluctuations. This multi-scale hydrogeochemical approach integrates complementary event-sensitive
103 methods, extending surface-hydrological tools such as C-Q analyses, and fill-and-spill and hotspot/hot moment concepts to a
104 subsurface mine drainage setting. Ultimately, this study contributes a transferable framework for diagnosing contaminant risks
105 in legacy mine settings and supports the development of adaptive, near-source water treatment strategies.

106 **2 Methods**

107 **2.1 Study site and sample collection**

108 Situated in the Ore Mountains of Central Europe, the historic Reiche Zeche mine site, 50.928° N 13.357° E, is one of the many
109 old mines whose runoff flows untreated into streams that feed the Elbe river, one of the largest rivers in Europe (LfULG,
110 2014). This site was active in extracting high-grade minerals, specifically silver ore, and processing mine waste rock up until
111 1969. The host rocks comprise mica schist and gneiss intersected by polymetallic sulfide-quartz-carbonate veins containing
112 pyrite, sphalerite, galena, and chalcopyrite, with minor arsenopyrite, barite, and fluorite (Baacke, 2001; Tichomirova et al.,
113 2010). These sulfide-rich assemblages are key sources of acid generation and metal mobilization, while secondary Fe-
114 (oxyhydr)oxides formed under drainage conditions contribute to local attenuation. Following mine decommission, the lower
115 sections of the adit system, which extend down to 1300 meters, became inundated with water up to the level of the central adit
116 “Rothschorberger Stolln”, which is accessible at approximately 230 meters below the surface at the Reiche Zeche mine shaft
117 (Zhiteneva et al., 2016; Mischo et al., 2021). The mine now represents a flooded, multi-level system with complex subsurface
118 flow pathways. This hydrological complexity, dispersed flow above extraction levels and preferential flow through waste
119 deposits, makes the site ideal for addressing our research questions.

120 This study focuses on a single slanted vertical extraction structure which spans over three levels before reaching the central
121 drainage adit (Fig. 1). These levels include: Level 1 (located 103 meters below the surface); Level 2 (149 meters below the
122 surface); and Level 3 (191 meters below the surface). A total of 26 sites were selected for ongoing sampling, but four specific
123 sites will be in the focus. The four locations, sites 1, 2, 3A, and 3B, were selected due to the presence of continuous and ample
124 amounts of flowing water in comparison to the rest of the locations which were not as great in volume of flowing water (see
125 images of four locations in Fig. S6). In one-to-three-week intervals, we conducted 42 sample campaigns to all sites from
126 February 3rd, 2022 to May 31st, 2024. All data are reported in the B2SHARE Data Repository (Sanchez et al., 2026).



127
128 **Figure 1: Conceptual framework and study layout of the abandoned mine system levels above the main adit at Reiche Zeche. Left:**
129 **monitoring locations across three mine levels, with four sites (1, 2, 3A, 3B) selected for high-frequency sampling. Instrumentation at**
130 **all four sites included flow loggers, with additional high-frequency sensors and an autosampler deployed at site 2 for a 10-month**
131 **intensive monitoring period. Middle: concept of site placement along flow path through the mine and associated contaminant**
132 **hotspots (blueish purple zones). Potential hotspots along the flow paths to sites 3A and 3B are depicted in different color shades to**
133 **emphasize their distinct source zones, despite spatial proximity to site 2. Right: conceptual model of flow-phase-dependent fill-and-**
134 **spill connectivity. Blue arrows represent flow direction; shaded red areas indicate stratification. Flow regimes govern activation of**
135 **solute source zones, resulting in distinct connectivity patterns.**

136 2.2 Sampling design and conceptualization of site-specific dynamics

137 To unravel the internal dynamic hydrogeochemical characteristics of the abandoned ore mine and to interpret observed
138 heterogeneity in space and time, we focused on the four sites, enabling a vertical profile of hydrological connectivity within
139 the system (Fig. 1). Over two years of sampling, we measured discharge, isotopic composition ($\delta^2\text{H}$ and $\delta^{18}\text{O}$), and dissolved
140 metal(lloid) concentrations at all 26 locations (Fig. 1 and Table S1). These measurements form the basis for subsequent analyses
141 described later on. Initial observations revealed strong spatial heterogeneity in metal(lloid) concentrations (Fig. S1) and
142 dynamic flow variability, which suggests the presence of transient contaminant hotspots and episodic connectivity. For a
143 process-based interpretation of these patterns, we developed a hotspot connectivity concept grounded in the fill-and-spill
144 paradigm (Fig. 1, right panel).

145 The Central European hydrological cycle (wet winters, dry summers) produces three recurring drainage phases in the mine:
146 flush (high flow), declining flow, and low flow. During low flow, hydrological disconnection allows solutes to accumulate in
147 lentic or weakly connected storage zones. Flush events re-establish connectivity, linking multiple pools and triggering
148 contaminant release (Sanchez et al., 2024), while declining flow reflects waning but still active transport. Stratification during

150 low and declining flows (Fig. 1) acts as a critical disconnection mechanism that can delay or abruptly initiate solute
151 mobilization.

152 Although sites 3A and 3B are located on the same mine level, they receive water from distinct source zones shaped by
153 geological structure, mining voids, and fracture networks. These differences lead to divergent C–Q dynamics and phases of
154 the fill-and-spill cycle, reflecting contrasts in pool storage, reconnection timing, and redox conditions. Such site-specific
155 variability underscores the need to analyze contaminant transport at multiple locations within the mine.

156 157 **2.3 Hydrological data collection and analysis**

158 To understand whether surface hydro-meteorological forcing translates into episodic contaminant release underground, we
159 monitored both external conditions and internal mine discharge. Meteorological conditions are monitored in an automated
160 station at the surface next to the central access shaft to the Reiche Zeche research and education mine. To avoid more complex
161 hydrological modelling, a standardized water availability index, i.e. the Self-Calibrating Palmer Drought Severity Index
162 (PDSI), was used to characterize the overall moisture conditions of the system and pre-event wetness levels (Wells et al., 2004;
163 Palmer et al., 2016). The PDSI (adhered to as water availability index) values are determined by using reference potential
164 evapotranspiration (FAO56 Penman-Monteith method) and precipitation data, and a simplified soil water balance model. This
165 accounts for both short-term fluctuations and long-term storage effects with its self-calibrating structure allowing the effective
166 storage capacity to adjust dynamically to the amplitude of the local weather variability. The magnitude of PDSI indicates the
167 severity of the departure from normal conditions. A PDSI value greater than 1 represents wet conditions, while a PDSI value
168 less than -1 represents dry conditions at the surface. The general dry and wet phases from the surface were compared with flow
169 rate measurements from within the mine.

170 Continuous water level and flow monitoring was conducted at four sites within the Reiche Zeche mine using pressure sensors
171 (Levelogger5, Solinst Georgetown) between February 2022 to March 2024. Sites 1 and 2 were equipped with plastic weirs for
172 discharge measurement, while the existing carved spillways were used at sites 3A and 3B. Site-specific water level-discharge
173 relationships were established (Henderson, 1966) and the resulting flow time series were smoothed using a Savitzky-Golay
174 filter.

175 Additionally, to distinguish between recharge and stored drainage contributions, water stable isotopes ($\delta^2\text{H}$ and $\delta^{18}\text{O}$) were
176 analyzed via cavity ring-down spectroscopy (L-2130i, Picarro Santa Clara) to trace water sources (See SI for details on
177 discharge calculations and isotope methods). Comparison with the local meteoric water line (LMWL) and calculation of an
178 offset from the general background concentration (centroid of all samples) and between the stations were used to assess
179 seasonal recharge and drainage contributions and distinguish between precipitation-dominated and older subsurface waters.

180 181 **2.4 Physico-chemical data collection and analysis**

182 To evaluate contaminant concentrations and solute composition, we combined field parameters with laboratory analyses. Acid-
183 washed HDPE bottles, pre-rinsed with deionized water, were used to collect water samples. For all samples, pH and

conductivity were measured (pH 340 and Cond 3310 sensors, WTW Weilheim). Prior to conducting analyses for dissolved organic carbon (DOC), dissolved inorganic carbon (DIC), and metal(loid)s, we filtered the samples using polyethersulfone filters with 0.45 µm pores (Filtropur S, Sarstedt Nümbrecht). The DIC and DOC concentrations were measured in triplicate for each sample using a total organic carbon analyzer (TOC-L series, Shimadzu Duisburg). For DOC measurements, we employed a high temperature combustion method, categorizing it as non-purgeable organic carbon (NPOC). This involved acidifying and then purging the samples with oxygen to expel inorganic carbon before the analysis. The precision of our data was validated by computing the standard deviation of the triple measurements, ensuring data reliability within the instrument's precision range (coefficient of variation < 2% and standard error < 0.1). We quantified metal(loid) concentrations using inductively coupled plasma optical emission spectroscopy (ICP-OES Optima 5300 DV Spectrometer, PerkinElmer Rodgau). For metal(loid) analysis, we prepared the samples with an addition of 1 mL of 2M nitric acid and included the following metal(loid)s in our analysis: iron (Fe), zinc (Zn), arsenic (As), copper (Cu), cadmium (Cd), lead (Pb), aluminum (Al), nickel (Ni), and manganese (Mn). These parameters allowed us to assess both geochemical conditions and contaminant levels under varying hydrological phases.

2.5 Automated sampling and high-resolution monitoring

To capture short-lived contaminant pulses that campaign sampling might miss, we complemented discrete sampling with automated high-frequency monitoring at site 2. An autosampler (6712 Full-Size portable sampler, ISCO Nebraska) was positioned at this site from May 16th, 2022 to February 14th, 2023 as an approach to avoid missing unseen aspects in the temporal dynamics of mine drainage water quality. The autosampler was calibrated to take a sample daily. 21 out of 24 1-L autosampler bottles were each filled with 10 mL of 2 M HCl prior to each start of the autosampler run to stabilize the metal(loid) solutions for measurements in the laboratory, while three autosampler bottles (one every seven days) were unacidified to record accurate pH and electrical conductivity measurements. The autosampler was filled every three weeks and 250 mL samples were collected from each bottle in the machine. Samples were filtered in the lab and prepared for further analyses. Prior to each new campaign, all 250 ml autosampler bottles were cleaned in a lab dishwasher and rinsed with deionized water. To complement this daily automated sampling, we submersed an online UV-Vis spectrometer probe (spectro::lyser V3, s::can GmbH Vienna; in the following simply termed spectrolyzer) in the flow channel from May 16th, 2022 to May 23rd, 2023 to record hourly absorbance measurements over a wavelength range of 200 to 720 nm at 2.5 nm increments.

To analyze and compare the spectral data obtained from the spectrolyzer with the metal(loid) concentration data collected by the autosampler at site 2 over time, we employed Quinlan's Cubist modeling (Kuhn and Johnson, 2013). Cubist, a rule-based method using spectrometric measurements, combines decision trees with linear models at the leaves, allowing for the prediction of continuous numerical variables. This approach was suited to our study because it handles non-linear relationships while maintaining interpretability. The modeling framework was applied to all analyzed metal(loid)s (see SI for details), while here we highlight cadmium as an illustrative example.

218 **2.6 Statistical and analytical framework**

219 **2.6.1 Hydrological phase classification**

220 To evaluate the influence of hydrological and geochemical drivers on contaminant mobilization, we divided the time series
221 into three hydrologically defined flow phases: low flow, flush, and declining flow. This classification was informed by
222 temporal patterns in discharge and water availability index values, observed consistently across the four monitoring sites.
223 Declining flow was characterized with the onset of dry conditions depicted by the water availability index turning negative.
224 Low flow marks the phase when the flow remains at very low rates although the surface system has started to recover from
225 the drying phase. Flush is defined by the onset of high discharge. The hydrological phases will be complemented with
226 geochemical phases later on.

227

228 **2.6.2 Pollution Load Index**

229 We further calculated the Pollution Load Index (PLI) to assess the cumulative level of metal(loid) contamination across the
230 four flow monitored locations. The PLI provides an aggregated measure of contamination by integration of the contamination
231 factors (CFs) of individual metal(loid)s, calculated as a ratio of observed metal(loid) concentrations to their respective
232 background reference values (Jahan and Strezov, 2018):

233
$$PLI = (CF1 \times CF2 \times CF3 \dots \times CFn)^{\frac{1}{n}} \quad (1)$$

234 where $CF = C_{\text{metal}}/C_{\text{background}}$, and n is the number of metal(loid)s considered. A $PLI > 1$ indicates pollution, whereas $PLI < 1$
235 implies no contamination (Tomlinson et al., 1980). Reference concentrations (for all metal(loid)s except Al) were derived from
236 average values in the Elbe river at the Magdeburg station, located near the midpoint of the river, for the year 2022, obtained
237 from FGG Elbe Data Portal (Datenportal der FGG Elbe, 2025). This evaluation allowed us to assess relative contamination
238 levels at specific locations in the mine against a representative background from a major regional river.

239

240 **2.6.3 Concentration-Discharge analysis and indices**

241 Concentration-discharge (C-Q) relationships were analyzed in \log_{10} - \log_{10} space to determine whether certain areas of the mine
242 disproportionately contribute specific metal(loid)s across the hydrological phases. The equation in \log_{10} - \log_{10} form used to
243 describe general patterns between discharge and concentration magnitudes is as follows (Knapp et al., 2020):

244
$$\log_{10}(C) = \log_{10}(a) + b \log_{10}(Q) \quad (2)$$

245 with C as the concentration, Q as the discharge, and a and b as the intercept and slope values. The slope (b) value of each C-
246 Q relationship was used as the primary metric to evaluate site-specific solute behavior (Fig. 2).

247 Negative slopes ($b < 0$) reflect source-limited dilution, as solute sources become insufficient at higher flows (Basu et al., 2010).
248 Positive slopes ($b > 0$) reflect enrichment, pointing to transport-limited mobilization driven by large solute stores and increased
249 hydrological mobilization of solutes during increased hydrological connectivity (Pohle et al., 2021; Balerna et al., 2021). Flat
250 or near-zero slopes indicate chemostatic conditions, where concentrations vary little despite any changes in flow.

251 To further distinguish chemostatic from chemodynamic conditions, we calculated the ratio of the coefficients of variation of
252 concentration and discharge (CV_c/CV_q). Following Musolff et al. (2015), chemostatic behavior is characterized by $-0.2 \leq b \leq$
253 0.2 and $CV_c/CV_q \leq 0.5$, whereas chemodynamic behavior corresponds to $-0.2 \leq b \leq 0.2$ and $CV_c/CV_q \geq 0.5$. Completely
254 chemostatic conditions occur only when $b \approx 0$ and $CV_c/CV_q \ll 0.5$. While we adopt conventional thresholds as diagnostic
255 guides, this term is used in our phase scheme to refer to segments whose behavior tends towards chemostatic-like signatures.
256 To capture dynamic transport mechanisms, we additionally evaluated hysteresis in C-Q space using hysteresis index (HI)
257 methods developed by Lloyd et al. (2016), Zuecco et al. (2016), and Roberts et al. 2023. Lloyd et al. (2016) was used as a
258 directional index quantifying whether concentration responds earlier or later than discharge, while Zuecco et al. (2016) is an
259 angle-based method that incorporates both discharge and magnitude of the loop, capturing asymmetry between rising and
260 falling limbs. The HARP (Hysteresis Area, Residual, and Peaks) method from Roberts et al. (2023) provided a multi-
261 component description of hysteresis area, lag symmetry, and peak timing, enabling a more holistic characterization of event-
262 scale transport behavior. metrics for the hysteresis analysis. (Methodological details are included in the SI).
263 Hysteresis patterns reveal time lags between discharge and concentration, offering insights into hydraulic connectivity (Pohle
264 et al., 2021) and mobilization processes at large (Lloyd et al., 2016). HI values typically range from -1 to +1, with positive
265 values indicating clockwise hysteresis and negative values indicating counterclockwise hysteresis (Vaughan et al., 2017).
266 Interpretation depends on the underlying C-Q behavior, whether concentrations rise or fall relative to discharge, and the
267 hydrological context. Thus, hysteresis patterns were evaluated jointly with slope and CV_c/CV_q ratios.
268 Together, these indices support systematic identification of shifts in contaminant sources, mobilization mechanisms, and
269 hydrogeochemical memory, and form the basis for our specific C-Q conceptualization and geochemical phase classification.
270

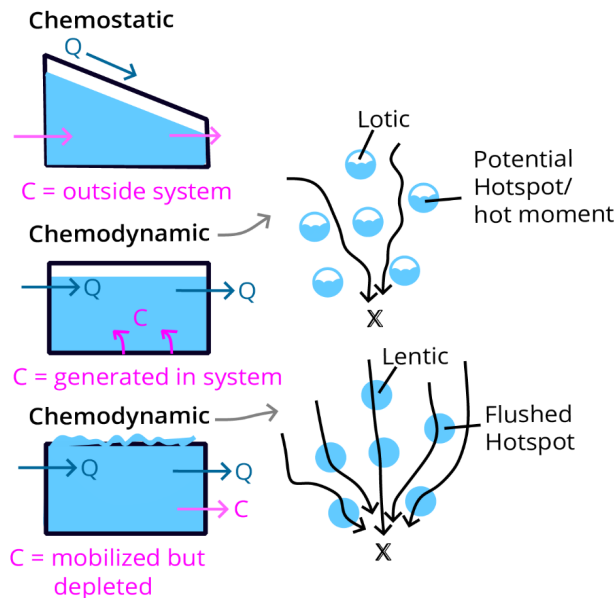
272 **2.6.4 Conceptualization of site-specific C-Q patterns**

273 In order to interpret the event-scale hydrodynamics in our system, a conceptual basis is needed as flow response analyses alone
274 do not fully capture the mechanistic processes that govern the supply of solutes to flowing waters. Observing C-Q dynamics
275 through a connectivity-mediated lens (Fig. 2a) enables the identification of episodic transitions and characteristics that extend
276 beyond general percolation and link to chemostatic and chemodynamic behaviors. Such transitions are best understood through
277 the fill-and-spill concept in which water accumulates in isolated pools until a threshold is reached, after which overflow
278 activates previously disconnected pathways (McDonnell et al., 2021). In our mine system, this behavior is further influenced
279 by lentic-lotic cycling, where solute accumulation occurs during lotic channelized low flow conditions that maintain prolonged
280 contact with metal-rich surfaces, followed by a transition to lentic, stratified pooling as water backs up behind internal
281 thresholds. When these lentic layers spill, connectivity is abruptly re-established and stored solutes are rapidly flushed from
282 the system, generating short-lived mobilization events (Schmadel et al., 2018). Depending on timing and degree of
283 connectivity, these activation events may or may not coincide with elevated contaminant loads.

284 Based on a point-to-point analysis of the C-Q dynamics for each solute and site, we observed distinct time dependent
 285 differences of how C-Q patterns evolved (Fig. 2b). Initial observations of hydrological flow and PLI patterns suggested four
 286 recurring sequence-based behaviors: loading, flushing, dilution, and recession. Episodes of chemostatic-like behavior (varying
 287 Q, stable C) also occurred, particularly during recession or periods of sustained connectivity. Here, our objective is not to
 288 assign phases solely from abstract C-Q quadrant patterns, but to identify when in the event sequence these behaviors emerge,
 289 and how they relate to underlying hydrological mechanisms such as threshold activation, lentic-lotic transitions, and fill-and-
 290 spill cycles.

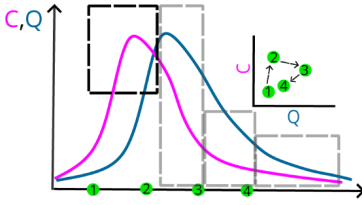
291

a) Concept hydrological dynamics

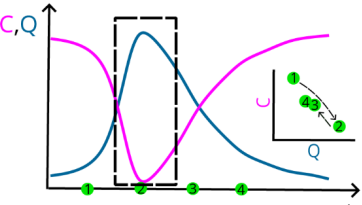


b) Event-scale geochemical patterns

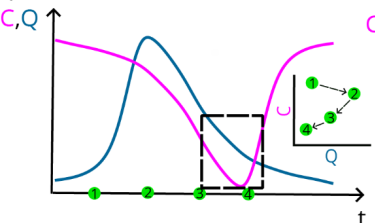
Loading: pools in lotic state build up loads and spill when flow/connectivity gets high



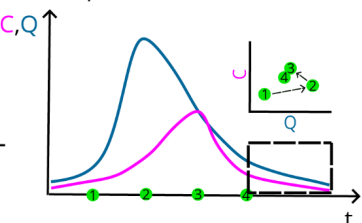
Flushing: rapid contaminant release without replenishing in lentic state



Recession: declines in Q and C precede reducing connectivity potential shift from lentic to lotic



Dilution: declining C and Q still sufficiently lentic to prevent a build up of contaminants



292

293 **Figure 2: (a) Conceptual representation of source and pool behavior with three dominant solute conditions. 1. External source input,**
 294 *where concentrations (C) remain constant across a range of flows (Q) 2. Internal generation, where solutes accumulate within isolated*
 295 *or weakly connected pools (e.g., lotic compartments) 3. Depleted pools, where previously enriched water masses are mobilized but*
 296 *concentrations progressively decline as storage is exhausted. (b) Event-scale co-evolution of concentration and discharge. Time-*
 297 *series patterns show loading, flushing, dilution, and recession patterns emerge during an event. Dark dotted box regions highlight*
 298 *time windows in which the certain behavior is observed. Light dotted box regions in the first C-Q plot are shown to acknowledge*
 299 *that other behaviors may also be present throughout different time points. Consecutive observations (green points) illustrate how*
 300 *these patterns evolve through a hydrological event, and these transitions reflect the interplay of fill-and-spill activation, lentic-lotic*
 301 *switching, and the spatial distribution of internal solute reservoirs. Together, these panels illustrate how event-driven changes in*
 302 *connectivity and solute availability produce contaminant export behavior, including short-lived hotspots and hot moments.*

303

304 Applying traditional C-Q relationships in this temporal point-wise manner allows us to reveal how phase transitions structure
305 contaminant export and generate hotspots of locally intensified metal release (Vidon et al., 2010) and hot moments of
306 intensified metal discharge. These event- and site-specific patterns provided a process-based understanding of solute
307 mobilization pathways that complemented the broader hydrological regime which aid in the development of our geochemical
308 phase framework.

310 **2.6.5 Geochemical phase classification**

311 In addition to the hydrologically defined phases, we introduced geochemically defined phases to resolve finer-scale temporal
312 variability in contaminant mobilization. To classify these phases, we examined time series trends in water availability index,
313 discharge, PLI, C-Q slope, CV_c/CV_q ratio, and HI behavior using the methods from Lloyd et al. (2016), Zuecco et al. (2016),
314 and Roberts et al. (2023) for each site. This multi-metric approach follows recent guidance by Knapp and Musolff (2024), who
315 emphasize that C-Q tools should not be interpreted in isolation but instead integrated with hydrological and geochemical
316 context to avoid overgeneralization. By manually evaluating these parameters together over time and developing an automated
317 classification algorithm, we identified characteristic patterns that delineate transitions between geochemical phases (Fig. S4).
318 To quantify the instantaneous C-Q behavior, each pair of consecutive observations were evaluated using a point-to-point
319 approach. For each segment, we calculated the C-Q slope and CV_c/CV_q ratio using a five-point rolling window, as well as the
320 hysteresis index values calculated on the time window surrounding each segment. These metrics were integrated into a
321 hierarchical rule-based classification algorithm in which each segment was assigned a confidence score (0-1) based on how
322 strongly its C-Q slope, CV_c/CV_q ratio, and hysteresis behavior matched characteristic patterns for each phase. Phases were
323 evaluated in priority order (flushing, loading, chemostatic, dilution, recession, and variable), with the first phase whose rules
324 triggered being selected as the dominant phase of that segment.

325 These phases were interpreted within the chemostatic-chemodynamic framework of Musolff et al. (2015), in conjunction with
326 the hydrological phase classification and the connectivity-based conceptual model (Fig. 2), ensuring that our phase
327 classifications aid in process-based interpretations of contaminant transport and mobility. From these combined trends, we
328 developed a working hypothesis in which these recurring geochemical phases emerge (Fig. S4):

- 329 1. Loading phase: Segments with increasing PLI values, negative C-Q slopes, and negative hysteresis during which flow is at
330 its low or increasing were classified as loading. These conditions reflect moments where water resides long enough in
331 isolated pools or channelized pathways for solute stores to accumulate. These segments correspond to the filling state before
332 threshold activation.
- 333 2. Flushing phase: Segments with initially high PLI values which lower as discharge increases, positive C-Q slopes, and
334 positive hysteresis were classified as flushing. These are short time windows where solute-rich lentic layers spill and
335 mobilize accumulated solutes as connectivity rapidly expands. This aligns with threshold exceedance and the activation of
336 previously disconnected domains.

337 3. Dilution phase: Segments with variably high flows and declining PLI values, and relatively high CV_c/CV_q ratios with
338 positive hysteresis were classified as dilution. Here, solute concentrations decrease due to mixing depleted lentic waters
339 and less solute-rich flow. Connectivity persists but source reservoirs become progressively exhausted.
340 4. Recession phase: Segments with lowering flow and stable or slightly declining PLI trends, very low CV_c/CV_q ratios, and
341 low water availability index values were classified as recession. These segments typically occurred during periods of
342 declining flow when connectivity contracts and solute exchange with source zones is limited.
343 5. Chemostatic: Periods where flow slightly varied but PLI, C-Q slope, and CV_c/CV_q ratios remained relatively stable with
344 low $CV_c/CV_q (< 1)$ and flat C-Q slopes, and low hysteresis indices were identified as chemostatic. These episodes occurred
345 during sustained connectivity when reactive surfaces remain buffered and concentrations change minimally.
346 6. Variable sources: Segments that did not match the characteristic patterns of other phases, typically showing relatively stable
347 flow and PLI trends with mixed or ambiguous changes in C-Q metrics were classified as variable sources. These segments
348 indicated solute dynamics driven by processes other than flow magnitude alone.
349 Finally, points of maximum pollution potential were further identified where high concentrations were reached before
350 transitioning to a substantial dilution behavior. These points represent the likely onset of a hot moment in contaminant
351 mobilization. By integrating hydrological flow and PLI trends with point-wise C-Q evolution, fill-and-spill behavior, and
352 lentic-lotic transitions, this phase classification and framework provides a mechanistic basis for interpreting episodic solute
353 mobilization in underground mine systems.

354 2.6.6 Data visualization

355 All figures and data visualizations were produced using Python (v3.12), primarily with the pandas (McKinney, 2010; pandas
356 development team, 2020) and plotly (Plotly Technologies Inc., 2015) libraries, and are reproducible with the code in the dataset
357 (see Sanchez et al., 2026) and the code for the geochemical phase classification (Jackisch and Sanchez, 2026). The conceptual
358 frameworks outlined in Fig. 1 and 2 further guided our analysis, motivating the structure of the results to follow the dynamics
359 of flow-phase-dependent connectivity and site-specific contaminant mobilization.

361 3 Results and discussion

362 3.1 Spatial and temporal patterns in hydrological and geochemical parameters

363 The hydrological regime of the Reiche Zeche mine system exhibits pronounced temporal and spatial heterogeneity, driven by
364 internal storage thresholds and episodic connectivity. Figure 3 summarizes key surface and subsurface hydrologic indicators,
365 including the water availability index, precipitation, and discharge at the four monitored sites. Based on hydro-meteorological
366 observations, declining flow, low flow, and flush phases of the mine drainage dynamics were identified. The declining phase
367 is informed by the overall moisture regime starting with the landscape shift from wet to dry states and ending when both flow
368 and dryness reach their minimum. These patterns were observed for two annual cycles (i.e. in 2022 and 2023). Notably, flush
369 phases occurred in February 2023 – May 2023 and December 2023 – February 2024, marked by sharp increases in discharge

370 across all four sites. Discharge trends did not align tightly with precipitation inputs, suggesting delayed and non-linear
371 hydrological responses (Milly et al., 2002; Bales et al., 2018). Direct reactions to surface storm events are very rare (Burnt et
372 al., 2025) such that, although surface conditions transitioned from drought to wetter periods in early autumn, increased mine
373 water discharge only became evident months later.

374 This temporal disconnect may reflect both delayed percolation to deeper layers and threshold-based fill-and-spill dynamics
375 within vertically structured storage zones. The more pronounced discharge peaks observed at deeper sites (i.e., sites 3A and
376 3B) compared to shallower sites closer to the surface (i.e., site 1; Li et al., 2022) suggest that connectivity is not continuously
377 active, but rather modulated by threshold exceedance, consistent with a fill-and-spill mechanism. The materials within these
378 contaminant stores are easily entrained once hydrologic thresholds are crossed (e.g., rising water tables or shear stress
379 increases), leading to a sharp but short-lived release pulse (Resongles et al., 2015). This illustrates how flow-phase-dependent
380 changes in hydrological connectivity control source zone activation. Similar to braiding rivers, we expect parts of the system
381 as being always drained and an increasing number of adjacent pools becoming connected with increasing water flow (Wilson
382 et al., 2024). Permanently spilled sections have rather low metal(loid) concentrations, while temporarily disconnected sections
383 act as niches for microbially mediated solving and hence elevated metal(loid) concentrations (Sanchez et al., 2025).

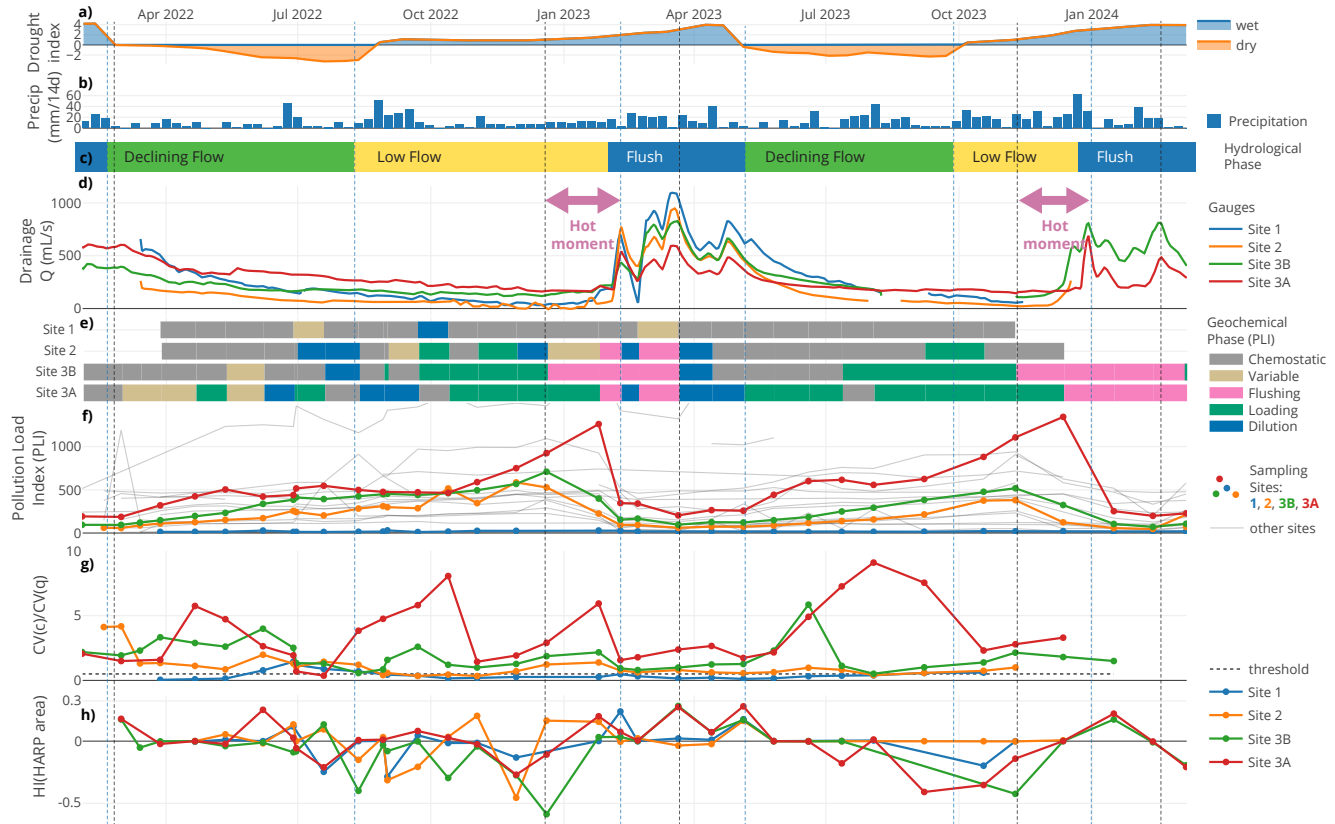
384 To further understand these patterns, we assessed spatial and temporal trends in the pollution load index (PLI) (Jahan and
385 Strezov, 2018), which integrates multiple dissolved metal(loid) concentrations into a single risk metric (Fig. 3f). The PLI time
386 series reveal clear site- and flow phase dependent variability. Notably, site 3A consistently exhibited the highest PLI values,
387 often exceeding a value of 500, well above the pollution threshold of one (Tomlinson et al., 1980). These elevated PLI values
388 declined sharply early in the flush events, consistent with dilution by low ionic strength water and enhanced mixing (Cánovas
389 et al., 2007), and further suggesting solute buildup during low connectivity followed by rapid export when flow paths are
390 reactivated.

391 We further classified the geochemical response at each site into distinct phases reflecting shifts in source zone activation and
392 storage-release dynamics. These phases, derived from C-Q relationships and aligned with hydrologically defined flow
393 conditions, include loading (characterized by temporal increases in solute concentration during low flow), flushing (rapid
394 contaminant release upon reactivation), and dilution (declining concentrations with rising discharge). Additional phases
395 include recession (post-flush declines in both flow and solute levels), chemostatic behavior (varying discharge with relatively
396 stable concentrations), and variable phases (mixed or unstable transport conditions). This phase-based framework, illustrated
397 by using PLI trajectories (Fig. 3e-f), offers a dynamic perspective on how internal thresholds and subsurface connectivity shifts
398 modulate contaminant export, which is not in phase with the discharge dynamics. This approach challenges traditional
399 drainage-based hypotheses by revealing that solute export is not a continuous seepage process, but rather a sequence of non-
400 linear mobilization events tied to internal storage activation.

401 Site-specific patterns highlight important contrasts in system behavior. While site 1 (located on level 1 at 103 m below surface
402 in our underground mine system) exhibited muted responses with the lowest PLI values, suggesting this point to depict the
403 water entry into the subsurface deposit structures, sites 2, 3A, and 3B exhibited stronger temporal variability, indicative of

reactive source zones. In the lead-up to flushing events, elevated dissolved metal(lloid) concentrations suggest slow leaching or desorption during storage-dominated phases (Pohle et al., 2021; Speir et al., 2024), while post-flush declines point to transient depletion of pools. CV_c/CV_q ratios (Fig. 3g) reveal mostly chemodynamic behavior at sites 2, 3A, and 3B, with sharp peaks preceding flushing events and indicating unstable solute supply as connectivity expands. Correspondingly, large HARP hysteresis areas at these sites (Fig. 3h) reflect repeated short-lived mismatches between concentration and discharge, reflecting rapid shifts between lentic and lotic states. These sharp fluctuations in PLI and C-Q metrics and synchronized concentration responses (Fig. S1) highlight the episodic nature of contaminant release and support the view that reconnecting flow paths mobilize previously isolated geochemical reservoirs.

412
413



414
415
416
417
418
419

Figure 3: Water and metal transport regime in the Reiche Zeche mine. (a) Dryness index as an indicator of the general water situation on the surface. (b) Weekly precipitation collected from Reiche Zeche, Freiberg weather station. (c) Hydrologically defined flow phases. (d) Discharge at the four sites in the Reiche Zeche mine. Pink arrows represent time periods when hot moments occur. (e) Geochemical hysteresis phases of pollution load index (PLI) at the four sites. Recession phase is not shown since it was not identified in the analysis. (f) PLI dynamics, (g) CV_c/CV_q ratios (with a threshold of 0.5), and (h) Hysteresis Area from the HARP

420 method are shown across the mine system. Individual sites are connected by black lines and colored lines are monitored flow sites
421 for sites 1, 2, 3A, and 3B.

422

423 3.2 Trends in metal load patterns and isotopic deviations

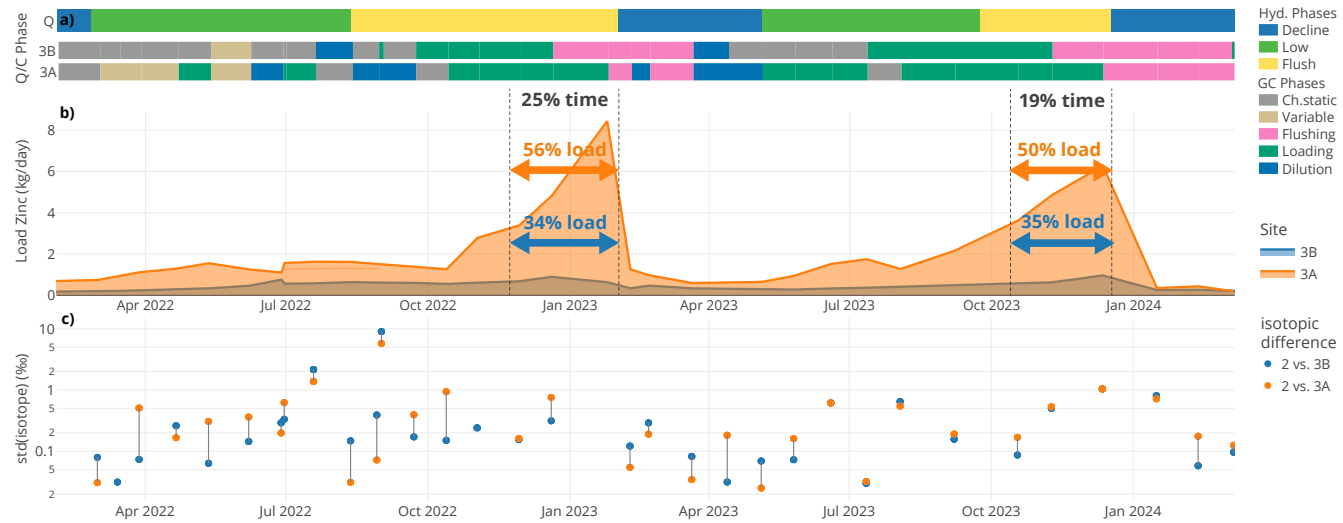
424 While PLI values present a general overview of metal(loid) behavior, looking into metal specific load dynamics (Fig. S3)
425 revealed key insights into the mechanisms controlling contaminant release in legacy mine systems. The daily Zn load (in terms
426 of flux, i.e. concentration times discharge) patterns observed at sites 3A and 3B (Fig. 4) exhibit sharp Zn load peaks shortly
427 before major flushing events, despite relatively stable or declining discharge conditions. While these pre-flush peaks occurred
428 during hydrologically low flow phases at both sites, the sites differ in terms of the contribution of each geochemical phase
429 within their fill-and-spill dynamics, such that this is more pronounced for site 3A than for site 3B. At site 3B, Zn dynamics are
430 less consistent with threshold-driven mobilization, suggesting that additional processes, such as dilution by younger recharge
431 waters or stratified storage, may have played a role as well. In contrast, site 3A shows sharper peaks that are better explained
432 by threshold-exceedance behavior. Once Zn accumulation is at its peak and mobilization begins, Zn loads drop abruptly,
433 reflecting rapid dilution or depletion of accumulated pools. This suggests that site 3A may be a more important target for water
434 remediation.

435 Quantitatively, these short 2-3 month intervals account for 50-56% of the total annual Zn load at site 3A and 34-35% at site
436 3B, despite occupying less than 25% of the time period. This highlights a strong fill-and-spill style signature, where
437 contaminants accumulate gradually under low connectivity and are then exported in intense but brief mobilization events.
438 Importantly, the overlay of flow and geochemical phases emphasizes how metal mobilization is driven by the timing and
439 sequence of hydrological reconnection.

440 To assess whether these mobilization pulses reflect deeper subsurface activation, we examined deviations in stable water
441 isotope compositions ($\delta^{2\text{H}}$ and $\delta^{18\text{O}}$) between deeper sites (3A and 3B) and the shallower reference site 2 (Fig. 4c) as a
442 measure of hydrologic connectivity. Individual samples plotted similarly close to the overall mine water background and the
443 LMWL (Fig. S2), indicating only minor shifts in water sources and weathering interaction at this scale. However, large isotopic
444 differences, predominantly during low flow periods in 2022, support the hypothesis of weak connectivity and more isolated
445 subsurface storage compartments. These differences narrowed considerably during flush phases, indicating reactivation of
446 previously disconnected zones. Shorter distances among standard deviations further point to site 3A (or 3B) being influenced
447 by similar water sources as site 2 during flushing phases. These patterns extend prior applications of isotopic tracers beyond
448 surface water systems (Spangenberg et al., 2007; Hazen et al., 2002), demonstrating their value for characterizing episodic
449 hydrological activation and subsurface connectivity in mining environments.

450 These findings challenge the conventional focus on high-flow conditions as the primary drivers of contaminant export from
451 mining-impacted systems. While prior studies have highlighted the role of high flow in resuspending contaminated sediments
452 or altering water chemistry (e.g., via pH or redox shifts) (Hudson-Edwards et al., 1997; Dawson and Macklin, 1998), our
453 results point to a dominant role of low flow inputs from subsurface or groundwater sources. Unlike classical baseflow, typically

454 low in flow and constant in concentration, these low flow periods exhibited highly variable metal levels, indicating
 455 disproportionate contributions to contaminant loads from subsurface pools or intermittently connected sources. Similar
 456 conclusions have been drawn in other abandoned mine systems (Bryne et al., 2020), where metal fluxes were sustained or even
 457 amplified under low flow regimes, underscoring the need to reconsider assumptions about contaminant risk during non-
 458 flushing conditions.



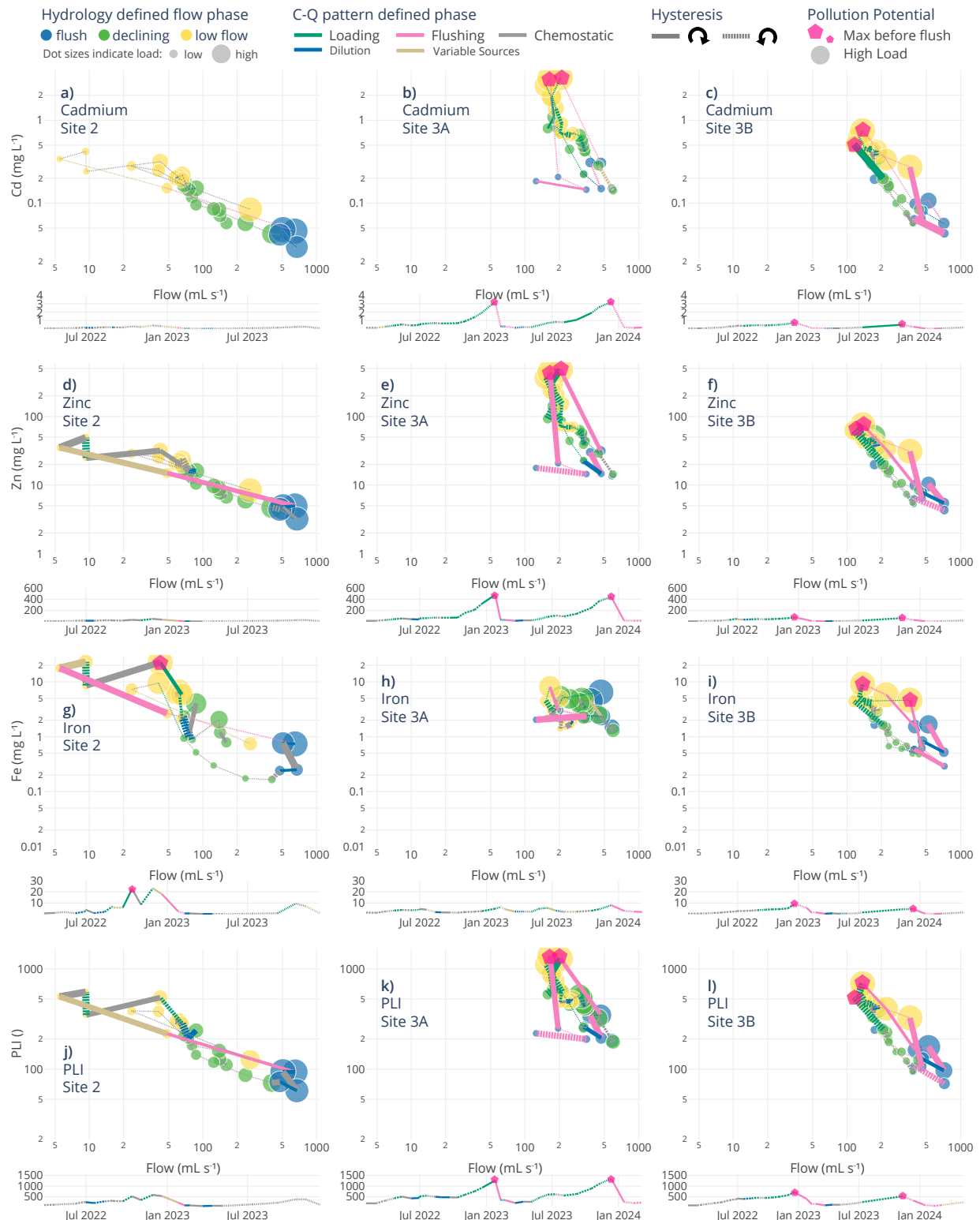
459
 460 **Figure 4: Zn loads and isotopic similarity from February 2022 to March 2024 are shown for sites 3A (orange) and 3B (blue). a)**
 461 hydrological phases (declining: green, low: yellow, flush: blue) and corresponding geochemical phases (e.g., loading, flushing,
 462 recession, dilution, and variable) for sites 3A and 3B (as in Fig. 3). b) Zn loads with peak load contributions labeled as percentages,
 463 indicating the proportion of total Zn export occurring in the 2-3 months preceding flushing. c) Standard deviation of isotopic
 464 concentrations ($\delta^{2\text{H}}$ and $\delta^{18\text{O}}$) to site 2. Difference between 3A and 3B marked as vertical lines. The relative ratio marks how much
 465 the water is similar (strong connection in flow field) or distinct (disperse paths) in the drainage system.

466
 467 The temporal synchronization of contaminant peaks across mine levels reveals a threshold-driven system governed by internal
 468 storage, episodic connectivity, and flow path structure. These processes collectively modulate metal(loid) transport and release,
 469 with site-specific patterns highlighting the role of delayed response and spatial heterogeneity in shaping contaminant export
 470 dynamics.

472 3.3 Dynamics in concentration-discharge relationships

473 Going beyond temporal and spatial trends, C-Q slopes (Table S3) provide insight into solute source proximity, mobilization
 474 timing, and hydrological connectivity (Knapp et al., 2020; Winter et al., 2021). Figure 5 presents diagnostic C-Q relationships
 475 for Cd, Zn, Fe and PLI at sites 2, 3A, and 3B, integrating hydrologically and geochemically defined phases. C-Q slopes
 476 (calculated for the entire sampling period) revealed very strong dilution patterns ($b < 0$) at sites 3A and 3B for Zn and Cd,
 477 which implies not only decreasing concentrations with increasing discharge but also a reduction in total solute loads compared

478 to the pre-flushing conditions. This suggests that at sites 3A and 3B incoming event water diluted the system more strongly
479 than metals were being mobilized, pointing to a depletion of readily exchangeable or previously accumulated solute pools.
480 One possible explanation is that during preceding low flow periods, metals accumulated locally but were not efficiently flushed
481 out during subsequent events, resulting in net declines in exported mass. In contrast, site 2 displayed a slope of -0.55, still
482 indicative of dilution but less pronounced, consistent with partial mobilization of stored solutes alongside dilution by incoming
483 recharge waters. These differences highlight that while all three sites show dilution-dominated behavior, the deeper sites (3A
484 and 3B) were characterized by stronger depletion, whereas site 2 retained evidence of ongoing solute mobilization events.
485 Within these general behaviors, we identified a “main pollution point”, the moment of peak concentration coinciding with
486 minimal discharge typically seen during the hydrologically defined low flow periods, highlighting a critical window of
487 contaminant risk. Eventually these points are followed by a shift to high flow and low concentration marked by dilution.
488 Segment-scale C-Q analysis further clarified how internal storage and release differ among sites. Across all metals at these
489 main pollution points, CV_c/CV_q ratios generally exceeded 0.5, and HI values consistently exhibited counterclockwise loops,
490 confirming that concentration variability is chemodynamic and governed by time-lagged storage-release dynamics, not
491 discharge magnitude alone. At site 3A, the combination of steep negative slopes and elevated CV_c/CV_q values (up to ~6)
492 indicates deep, isolated pockets of solute-rich water undergoing intense build up during low flow and abrupt depletion upon
493 early stage flushing. Site 3B exhibited similar but less extreme patterns, suggesting pools that accumulate solutes during quiet
494 periods but are shallower or refreshed more frequently. In contrast, site 2 showed the weakest dilution yet remained
495 chemodynamic, supporting the interpretation that this nearer to surface channel receives a continuous supply of water, allowing
496 only partial flushing of stored solutes.
497 When evaluated alongside the timing of pollution potential points, the data reveal that each site expresses hot moments through
498 different mechanisms. At site 3A this is through rapid collapse of deep, enriched pools and at site 3B through more moderate,
499 short-lived spikes, and at site 2 through smaller concentration peaks. Collectively, these site-specific differences underscore
500 how the location, connectivity, and hydrodynamic activation of contaminant-rich zones govern release dynamics, highlighting
501 that standard outlet-based monitoring may overlook episodic contributions from deeper, disconnected compartments. This has
502 direct implications for the design of monitoring strategies and for timing interventions to capture or mitigate short-lived
503 contaminant pulses.



505 **Figure 5: Concentration–discharge (C–Q) relationships (log₁₀ scaled) for (a–c) dissolved Cd, (d–f) dissolved Zn, (g–i) dissolved Fe, 506 and (j–l) Pollution Load Index at Site 2 (a, d, g, j), Site 3A (b, e, h, k) and Site 3B (c, f, i, l) during the three hydrologically defined 507 phases (flush – blue, declining – green, and low – yellow). Bright pink pentagon-shaped points are the main pollution points (i.e., 508 moments when high contaminant potential and high load is identified). Dot size represents the respective load. Under each C–Q 509 plot, the dissolved metal concentration and PLI values are shown across a time scale. The geochemically defined phase from the C–Q 510 patterns is represented through the color of the lines connecting each point for the C–Q plots with the line thickness corresponding 511 to absolute hysteresis index (Zuecco et al., 2016) and is distinguished by its direction (negative or near-zero HI dashed, positive HI 512 solid). This phase distinction is also shown for the time series with marked main pollution points.**

513
514 These short-term C–Q transitions observed across the sites map directly into the geochemically defined phases. The strongly
515 negative C–Q slopes observed at sites 3A and 3B occurred during our defined loading phase before the onset of flushing. These
516 segments reflect solute accumulation during low flow followed by a rapid decline in concentrations as connectivity begins to
517 increase, consistent with a system that has accumulated solutes in lotic pathways but is not yet connected enough for flushing.
518 As discharge begins to rise and thresholds are crossed, the system transitions into the flushing phase, marked by rapid release
519 of solute-rich waters from lentic pools. These flushing periods were generally shorter-lived compared to loading periods.
520 Following flushing, the system rapidly enters the dilution phase, where connectivity remains high, but solute stores become
521 limited. Concentrations continue to decrease but with comparably less negative C–Q slopes than those seen during the loading
522 phase, reflecting source-limited dilution in a partially lentic system. Notably, recent work has shown that C–Q slopes can
523 diverge substantially between event-scale and long-term observations (Winter et al., 2024), underscoring the importance of
524 analyzing C–Q relationships at short timescales using high-frequency data. During the later portions of events, we anticipated
525 recession phases to emerge, but within our automated classification, chemostatic-like conditions were more prominent at sites
526 2 and 3A, pointing to similar characteristic behavior of these two phases in which the system transitions back toward reduced
527 connectivity.

528 Importantly, while these classifications provide a coherent and mechanistic lens for interpreting short-term hydrogeochemical
529 behavior, we view them as guiding tools rather than fixed or exhaustive categories. This aligns with recent discussions (e.g.,
530 Knapp and Musolff, 2024) emphasizing that C–Q based frameworks, even when combined with additional metrics, cannot
531 capture all processes in complex subsurface environments. Thus, our framework serves as a structured interpretive aid
532 highlighting dominant patterns and the threshold-driven transitions in this mine system, where lotic-lentic and fill-and-spill
533 cycles jointly produce hotspots and hot moments of contaminant release.

534

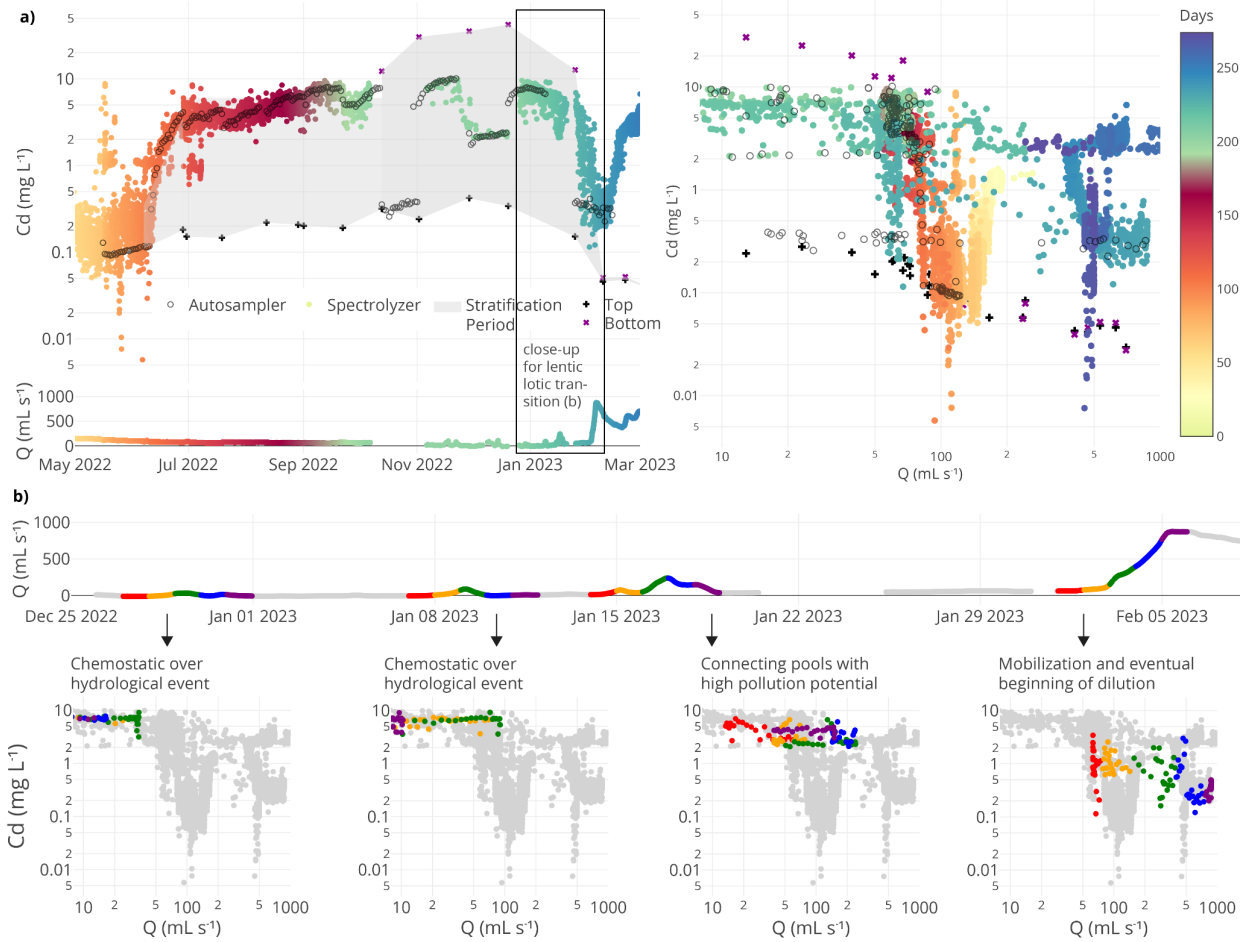
535 **3.4 Identification of high contaminant potential through spectrometric data**

536 To complement this integrative view from the tri-weekly sampling and to zoom into the transition from loading to mobilization,
537 we applied high-frequency monitoring with an in-situ UV-Vis spectrometer (collecting hourly measurements) and daily
538 autosampling at site 2. At site 2, a drainage channel with rough bottom structure creates a specific dynamic flow environment
539 where stratification, density contrasts, and throughflow coexist (Sanchez et al., 2025). This setting created a labile 2-phase

540 system: a low-density surface layer forming a hydraulically connected stream above a dense, metal-enriched bottom pool.
541 Such dual compartments acted as both storage and release zones, with stratification intermittently buffering and then abruptly
542 mobilizing contaminants. To capture these dynamics, we combined autosampler-based laboratory measurements with high-
543 frequency spectrometric estimates of dissolved Cd (Fig. 6). This dual approach revealed that transitions from solute
544 accumulation to flushing occurred within hours and much more rapid than what can be resolved by sampling alone,
545 highlighting short-lived but significant windows of contaminant export.

546 All monitoring methods consistently showed Cd buildup during low and declining flow (July – December), followed by sharp
547 concentration drops at the onset of flushing conditions. These shifts reinforce the role of threshold-based activation and
548 transient hydrological connectivity in controlling solute mobilization. In addition to these processes, the dynamics are also
549 consistent with gradual solute accumulation under density-stratified conditions followed by abrupt dilution conditions once
550 connectivity is established. Notably, stratification observed visually in mid-October 2022 to late January revealed Cd
551 concentrations in bottom grab samples (positioned near the channel base) more than two orders of magnitude higher than top
552 grab samples (collected at the surface). The grey polygon (i.e., grab sample corridor) in Fig. 6a delineates the concentration
553 range captured by these paired depth-integrated manual grab samples, as well as the spectrolyzer results over the low flow
554 period, providing a window into the presence of density-stabilized, solute-rich bottom waters. These findings suggest
555 temporary solute traps forming during quiescent conditions, a phenomenon also reported in mine systems with intermediate
556 density layering that can be rapidly flushed upon reactivation (Mugova and Wolkersdorfer, 2022; Mugova and Wolkersdorfer,
557 2024).

558 Figure 6b illustrates how phase-specific C-Q relationships for dissolved Cd evolved during a six-week period leading up to
559 the major flushing event in February 2023. Hourly data revealed shifting mobilization regimes, with clear transitions between
560 chemostatic and chemodynamic behavior, just before hydrological shifts. Each C-Q panel corresponds to a high-resolution sub
561 window from the flow time series, capturing short-lived events with discrete geochemical responses. This highlights how
562 although during small or intermediate increases in flow, characteristics of chemostatic conditions may prevail, in a short time
563 span these conditions can change and be initiated from accumulated solute pools, especially under stratified or semi-stratified
564 conditions where density-driven segregation creates temporary storage zones. During low to moderate flow conditions, even
565 minor discharge increases can lead to the buildup prior to contaminant mobilization when residual sources remain available,
566 eroding micro-stratification and reconnecting isolated pools with high pollution potential. In contrast, during high flow
567 conditions, when temporary storages are already exhausted, these pools may be heavily mobilized, such that a variability of
568 dilution, loading, and recession typically dominate the C-Q relationship (Fig. 6b, ‘Mobilization and eventual beginning of
569 dilution’ panel). Solute transport regimes transition within just a few days to weeks as discharge fluctuates, underscoring the
570 dynamic connectivity of source zones and complements the broader patterns seen across sites and metals in Fig. 5. These
571 findings reinforce that episodic hydrological forcing can lead to metal-specific, rapidly evolving export regimes that cannot be
572 captured by temporal sampling alone. Our results further illustrate how event-scale monitoring captures transient transport
573 processes that could be obscured in analyses based solely on long-term, low-frequency data.



574

575 **Figure 6: (a) Top right panel: Dissolved Cd concentrations (log₁₀ scaled) at site 2 measured using an autosampler (daily values in**
 576 **577 open circles), the spectrometer instrument (hourly values in colored circles), and manual sampling (bottom - purple crosses; top -**
 578 **black crosses). The grab sample corridor (grey polygon) represents the concentration range in which stratification was evident based**
 579 **on all sampling methods (until stratification collapse). The spectrometer measurements are colored by sampling day to indicate**
 580 **temporal regression. The black box with the annotation of close-up for lentic-lotic transition highlights the six-week window analyzed**
 581 **in detail in panel b. Bottom panel: The time series for the water discharge matching with the spectrometer color scheme. Top left**
 582 **583 panel: C-Q relationship (log₁₀ scaled) for dissolved Cd following the same spectrometer color scheme as the right panel. (b) Top panel:**
 584 **The time series of the six-week window for the discharge matching with the spectrometer color scheme. Bottom panels: Phase-**
 585 **586 resolved C-Q patterns (log₁₀ scaled) for dissolved Cd over the stratification-collapse and lentic-lotic transition. Each small C-Q panel**
 587 **588 shows hourly Cd-Q data for a 5-day segment, with points colored by each day (day 1 - red, day 2 - orange, day 3 - green, day 4 -**
 589 **blue, day 5 - purple). C-Q plots highlight progressive phases in the transition between lentic to lotic or fill to spill conditions. After**
 590 **591 the first two hydrological events showing chemostatic characteristics (2022-12-27 to 2022-12-31 and 2023-01-07 to 2023-01-11), the**
 592 **593 third event hints to connecting pools with high pollution potential (2023-01-14 to 2023-01-18), which are eventually mobilized in the**

588 **fourth and strongest breakthrough event mobilization (2023-02-01 to 2023-02-05). These panels are linked to their respective periods**
589 **in the hourly discharge time series.**

591 The combined use of autosampler and high-frequency spectrolyzer data offer synergistic insights, such that the former anchors
592 the dataset in analytical accuracy, while the latter captures transient solute behavior and enables time-resolved analysis of
593 flow-phase transitions. This integrated perspective, alongside zooming into small time windows of C-Q responses, is critical
594 for detecting and characterizing hot moments, in which brief but disproportionate pulses of metal export can dominate annual
595 metal loads. Our findings emphasize that stratified pools stabilized during low flow can be rapidly activated within a short
596 window during fill-and-spill (McDonnell et al., 2021) or lentic-lotic cycle transitions (Shaw et al., 2020), reinforcing the need
597 for depth-aware, event-sensitive monitoring to anticipate episodic contaminant risks in complex mining systems.

598

599 **3.5 Implications for contaminant pollution remediation**

600 Our findings highlight that contaminant mobilization in abandoned mine systems is not primarily driven by storm intensity or
601 seasonal high flows, but by internal hydrological thresholds and episodic connectivity between stored contaminant pools and
602 the active drainage network. The observed lag between peak accumulation and flushing, followed by rapid load collapse,
603 suggests that predictive assessments must incorporate not just hydrometeorological variables but also the internal memory of
604 the system.

605 These dynamics expose critical blind spots in current water quality monitoring and regulatory frameworks. Existing
606 benchmarks, such as German sediment quality guidelines (e.g., 800 mg/kg Zn in suspended materials) (Bundesamt für Justiz,
607 2016) and EU background dissolved Zn concentrations (1–35 µg/L) (Munn et al., 2010; Comber et al., 2008) overlook the
608 timing and intensity of short-lived, high-risk release events from underground contaminant reservoirs. Figures 5 and 6 illustrate
609 this clearly. Figure 5 provides a system-scale diagnostic, showing how metals and PLI evolve across sites and flow phases,
610 with highlighted hot moments pinpointing pulses that carry disproportionate contaminant loads. Figure 6 then zooms in at high
611 temporal resolution, capturing the collapse of stratification and lentic-lotic transition that triggered a breakthrough event.
612 Therefore, the hot moments of release, which arise during hydrologically quiet intervals rather than extreme events, may
613 represent important windows of strategic intervention.

614 While this study focuses on the Reiche Zeche mine, the fill-and-spill dynamics we observe are likely widespread across
615 hydrologically complex, mining-impacted systems, especially in porous systems with variable subsurface connectivity,
616 stratified drainage zones, or episodic flow regimes. Similar mechanisms may be active in karst aquifers, tunnel-fed drainages,
617 or engineered infrastructure where discrete contaminant pools are intermittently connected to surface outflows. This shift from
618 peak flow emphasis in such systems toward detecting internal system thresholds supports a more proactive, precise, and
619 strategic path for better timed remediation. Effective mitigation depends on anticipating these moments before widespread
620 flushing, when contaminant concentrations are high but spatially contained.

621 At site 3A, located near the central drainage adit and consistently exhibiting the highest PLI values, we observed Zn loads up
622 to 8.4 kg/day prior to a major flush event (mean 1.9 kg/day). This site contributes only 0.06% of the overall water to the outlet
623 of the overall adit Roths Schönberger Stolln, but 1.3% of the Zn load in average (LfULG, 2014) with the few days before flushing
624 accounting for about 50% of the annual load from flux-based metrics. While a more detailed monitoring using a spectrometer
625 at site 3A would have been advantageous, this comparison underscores that substantial contaminant fluxes can accumulate and
626 be released from within the mine system itself, often remaining undetected by conventional downstream monitoring. By
627 combining C-Q relationships and hysteresis analysis, our approach pinpoints internal hotspots and identifies hot moments of
628 high mobilization risk, advancing a framework to guide targeted monitoring and early-warning systems. Beyond this study,
629 these findings highlight the broader relevance of upstream diagnostics for understanding contaminant behavior in legacy mine
630 settings and support the need for spatially resolved, phase-sensitive strategies for remediation planning. The latter could include
631 specific small-scale treatment systems near to the actual mobilization hotspots in the legacy mines.

632 While our results emphasize the value of identifying internal hotspots and hot moments, remediation strategies involve clear
633 trade-offs. End-of-pipe treatments (e.g., treatment at mine outlets) offer practical advantages because they can operate as a
634 single, accessible location and do not require detailed knowledge of internal connectivity, but they may miss short-lived
635 contaminant pulses generated upstream. Source-proximal or hotspot-focused interventions can intercept highly concentrated
636 releases earlier, yet risk overlooking additional, undetected hotspots in hydrologically complex systems. Given that
637 contaminant mobilization is highly dynamic and rarely captured in current monitoring frameworks, an effective remediation
638 strategy likely requires combining system-scale and end-of-pipe safeguards with targeted upstream diagnostics to balance
639 feasibility with responsiveness to episodic release events.

640

641 **4 Conclusions**

642 This study demonstrates that contaminant mobilization in abandoned mine systems is controlled not by steady seepage but by
643 episodic shifts in internal hydrological connectivity. Across the Reiche Zeche mine, low flow and pre-flush phases were shown
644 to concentrate dissolved metal(loid)s in poorly connected storage zones, with subsequent reconnection triggering sharp but
645 short-lived contaminant releases. Event-scale C-Q relationships and indices reveal that such hot moments of export account
646 for a disproportionate share of annual metal loads, emphasizing the need to move beyond traditional outlet-based monitoring.
647 Our findings highlight three key insights: First, low flow periods represent high risk intervals of solute accumulation,
648 challenging assumptions that contaminant risk is greatest only during floods or peak flows. Second, site-specific C-Q dynamics
649 demonstrate that contaminant export is shaped by rapid transitions between hydrogeochemical phases, capturing how internal
650 hotspots formed during low flow evolve into hot moments of connectivity-driven release. Third, targeted monitoring of
651 connectivity threshold provides a basis for early warning and site-specific and near-source interventions. By identifying
652 internal hotspots and the timing of mobilization events, this work establishes a transferable framework for diagnosing
653 contaminant risks in legacy mine settings. These insights support a shift toward event-sensitive, near-source remediation

654 strategies that prioritize internal system dynamics, offering more efficient and scalable alternatives to conventional end-of-
655 pipe treatment.

656

657 **Author contributions**

658 **A.A.S.**: Conceptualization, Methodology, Formal analysis, Investigation, Data curation, Writing-original draft, Writing-review
659 and editing. **M.P.L.**: Conceptualization, Supervision, Validation, Writing: review and editing. **S.A.**: Spectral data analysis,
660 online UV-Vis Spectrometer data curation. **S.H.**: Validation, Writing: review and editing. **C.J.**: Conceptualization,
661 Supervision, Hydrological and hysteresis analysis, Data visualization and curation, Original Writing-original draft, Writing:
662 review and editing.

663

664 **Data Availability Statement**

665 The dataset supporting this study is openly available via the B2SHARE data repository under the title LegacyMine_HydroGeo:
666 Dataset on the geochemical and hydrological dynamics in a historic mine system (Sanchez et al., 2026). It includes high-
667 resolution geochemical, isotopic, hydrological, and spectrometric data collected from the Reiche Zeche mine over a two-year
668 monitoring period. The dataset can be accessed at <https://doi.org/10.23728/b2share.566z6-gtm46> and the geochemical phase
669 classification suite is available at <https://doi.org/10.5281/zenodo.1846291>.

670

671 **Competing interests**

672 The authors declare that they have no conflict of interest.

673

674 **Acknowledgements**

675 This research was conducted as part of the project "Source Related Control and Treatment of Saxon Mining Water" and was
676 funded by the Dr. Erich-Krüger Foundation. We extend our gratitude to Dr. Alexander Pleßow for his support with laboratory
677 equipment. Special thanks to Prof. Helmut Mischo and Stephan Leibelt for their training and access to the Reiche Zeche mine,
678 as well as to Dr. Andreas Kluge and Dr. Nils Hoth for their invaluable assistance in initiating work on the mine system. We
679 also wish to acknowledge the laboratory team—Thurit Tschöpe, Marius Stoll, Claudia Malz, Eva Fischer, and Lena
680 Grundmann—for their help with sample measurements, as well as Karl Haas and Lena Herzog for her assistance in collecting
681 mine water samples. We also thank Prof. Erwin Zehe and his team at KIT Karlsruhe for lending the ISCO autosampler.

682

683 **References**

684 Allen, D. M. and Voormeij, D. A.: Oxygen-18 and Deuterium Fingerprinting of Tailings Seepage at the Sullivan Mine, Mine
685 Water Environ., 21, 168–182, <https://doi.org/10.1007/s102300200041>, 2002.

686

687 Baacke, D.: Geochemical behavior of environmentally relevant elements in closed polysulphide ore pits using the example of
688 "Himmelfahrt" pit in Freiberg/Saxony. Dissertation, TU Bergakademie Freiberg, 2001.

689
690 Balerna, J. A., Melone, J. C., and Knee, K. L.: Using concentration-discharge relationships to identify influences on surface
691 and subsurface water chemistry along a watershed urbanization gradient, *Water (Switzerland)*, 13,
692 <https://doi.org/10.3390/w13050662>, 2021.

693
694 Bales, R. C., Goulden, M. L., Hunsaker, C. T., Conklin, M. H., Hartsough, P. C., O'Geen, A. T., Hopmans, J. W., and Safeeq,
695 M.: Mechanisms controlling the impact of multi-year drought on mountain hydrology, *Sci. Rep.*, 8, 690,
696 <https://doi.org/10.1038/s41598-017-19007-0>, 2018.

697
698 Basu, N. B., Destouni, G., Jawitz, J. W., Thompson, S. E., Loukinova, N. V., Darracq, A., Zanardo, S., Yaeger, M., Sivapalan,
699 M., Rinaldo, A., and Rao, P. S. C.: Nutrient loads exported from managed catchments reveal emergent biogeochemical
700 stationarity, *Geophys. Res. Lett.*, 37, <https://doi.org/10.1029/2010gl045168>, 2010.

701
702 Bozau, E., Licha, T., and Ließmann, W.: Hydrogeochemical characteristics of mine water in the Harz Mountains, Germany,
703 *Chemie der Erde*, 77, 614–624, <https://doi.org/10.1016/j.chemer.2017.10.001>, 2017.

704
705 Bundesamt für Justiz – Verordnung zum Schutz der Oberflächengewässer 1 Anlage 6: https://www.gesetze-im-internet.de/ogewv_2016/anlage_6.html, last access: 30 July 2025.

706
707 Burt, E. I., Allen, S. T., Braun, S., Tresch, S., Kirchner, J. W., and Goldsmith, G. R.: New Precipitation Is Scarce in Deep
708 Soils: Findings From 47 Forest Plots Spanning Switzerland, *Geophys. Res. Lett.*, 52, <https://doi.org/10.1029/2025gl115274>,
710 2025.

711
712 Byrne, P., Onnis, P., Runkel, R. L., Frau, I., Lynch, S. F. L., and Edwards, P.: Critical Shifts in Trace Metal Transport and
713 Remediation Performance under Future Low River Flows, *Environ. Sci. Technol.*, 54, 15742–15750,
714 <https://doi.org/10.1021/acs.est.0c04016>, 2020.

715
716 Byrne, P., Wood, P. J., and Reid, I.: The Impairment of River Systems by Metal Mine Contamination: A Review Including
717 Remediation Options, *Crit. Rev. Environ. Sci. Technol.*, 42, 2017–2077, <https://doi.org/10.1080/10643389.2011.574103>,
718 2012.

719
720 Cánovas, C. R., Olías, M., Nieto, J. M., Sarmiento, A. M., and Cerón, J. C.: Hydrogeochemical characteristics of the Tinto and
721 Odiel Rivers (SW Spain). Factors controlling metal contents, *Sci. Total Environ.*, 373, 363–382,
722 <https://doi.org/10.1016/j.scitotenv.2006.11.022>, 2007.

723
724 Clark, I. and Fritz, P. (1st Ed.): Environmental Isotopes in Hydrogeology, Lewis Publishers, New York, 342 pp., ISBN
725 9780429069574, 1997.

726
727 Comber, S. D. W., Merrington, G., Sturdy, L., Delbeke, K., and Assche, F. van: Copper and zinc water quality standards under
728 the EU Water Framework Directive: The use of a tiered approach to estimate the levels of failure, *Sci. Total Environ.*, 403,
729 12–22, <https://doi.org/10.1016/j.scitotenv.2008.05.017>, 2008.

730
731 Datenportal der FGG Elbe: https://elbe-datenportal.de/FisFggElbe/content/auswertung/MessstellenDetail_start, last
732 access: 11 July 2025.

733
734 Datta, B., Durand, F., Laforge, S., Prakash, O., Esfahani, H. K. , Chadalavada, S., and Naidu, R.: Preliminary Hydrogeologic
735 Modeling and Optimal Monitoring Network Design for a Contaminated Abandoned Mine Site Area: Application of Developed
736 Monitoring Network Design Software, *J. Water Resour. Prot.*, 08, 46–64, <https://doi.org/10.4236/jwarp.2016.81005>, 2016.

737

738 Dawson, E. J. and Macklin, M. G.: Speciation of heavy metals on suspended sediment under high flow conditions in the River
739 Aire, West Yorkshire, UK, *Hydrol. Process.*, 12, 1483–1494, [https://doi.org/10.1002/\(sici\)1099-1085\(199807\)12:9<1483::aid-hyp651>3.0.co;2-w](https://doi.org/10.1002/(sici)1099-1085(199807)12:9<1483::aid-hyp651>3.0.co;2-w), 1998.

741

742 Fovet, O., Belemougri, A., Boithias, L., Braud, I., Charlier, J., Cottet, M., Daudin, K., Dramaïs, G., Ducharme, A., Folton, N.,
743 Grippa, M., Hector, B., Kuppel, S., Coz, J. L., Legal, L., Martin, P., Moatar, F., Molénat, J., Probst, A., Riotte, J., Vidal, J.,
744 Vinatier, F., and Datry, T.: Intermittent rivers and ephemeral streams: Perspectives for critical zone science and research on
745 socio-ecosystems, *Wiley Interdiscip. Rev.: Water*, 8, <https://doi.org/10.1002/wat2.1523>, 2021.

746

747 Freeman, M. C., Pringle, C. M., and Jackson, C. R.: Hydrologic Connectivity and the Contribution of Stream Headwaters to
748 Ecological Integrity at Regional Scales 1, *JAWRA J. Am. Water Resour. Assoc.*, 43, 5–14, <https://doi.org/10.1111/j.1752-1688.2007.00002.x>, 2007.

749

750

751 Galván, L., Olías, M., Cánovas, C. R., Torres, E., Ayora, C., Nieto, J. M., and Sarmiento, A. M.: Refining the estimation of
752 metal loads dissolved in acid mine drainage by continuous monitoring of specific conductivity and water level, *Applied
753 Geochemistry*, 27, 1932–1943, <https://doi.org/10.1016/j.apgeochem.2012.07.011>, 2012.

754

755 Ghomshei, M. M. and Allen, D. M.: Potential application of oxygen-18 and deuterium in mining effluent and acid rock drainage
756 studies, Springer-Verlag, 2000.

757

758 Godsey, S. E., Kirchner, J. W., and Clow, D. W.: Concentration-discharge relationships reflect chemostatic characteristics of
759 US catchments, *Hydrological Processes*, 23, 1844–1864, <https://doi.org/10.1002/hyp.7315>, 2009.

760

761 Haferburg, G., Krichler, T., and Hedrich, S.: Prokaryotic communities in the historic silver mine Reiche Zeche, *Extremophiles*,
762 26, <https://doi.org/10.1007/s00792-021-01249-6>, 2022.

763

764 Hazen, J. M., Williams, M. W., Stover, B., and Wireman, M.: Characterisation of Acid Mine Drainage Using a Combination
765 of Hydrometric, Chemical and Isotopic Analyses, Mary Murphy Mine, Colorado, 2002.

766

767 Henderson, F. M.: *Open Channel Flow*, MacMillan, New York, 1966.

768

769 Herndon, E. M., Dere, A. L., Sullivan, P. L., Norris, D., Reynolds, B., and Brantley, S. L.: Landscape heterogeneity drives
770 contrasting concentration-discharge relationships in shale headwater catchments, *Hydrology and Earth System Sciences*, 19,
771 3333–3347, <https://doi.org/10.5194/hess-19-3333-2015>, 2015.

772

773 Huang, C., Guo, Z., Li, T., Xu, R., Peng, C., Gao, Z., and Zhong, L.: Source identification and migration fate of metal(lloid)s
774 in soil and groundwater from an abandoned Pb/Zn mine, *Science of the Total Environment*, 895,
775 <https://doi.org/10.1016/j.scitotenv.2023.165037>, 2023.

776

777 Hudson, E., Kulessa, B., Edwards, P., Williams, T., and Walsh, R.: Integrated Hydrological and Geophysical Characterisation
778 of Surface and Subsurface Water Contamination at Abandoned Metal Mines, *Water, Air, Soil Pollut.*, 229, 256,
779 <https://doi.org/10.1007/s11270-018-3880-4>, 2018.

780

781 Hudson-Edwards, K., Macklin, M., and Taylor, M.: Historic metal mining inputs to Tees river sediment, *Sci. Total Environ.*,
782 194, 437–445, [https://doi.org/10.1016/s0048-9697\(96\)05381-8](https://doi.org/10.1016/s0048-9697(96)05381-8), 1997.

783

784 Jackisch, C. and Sanchez, A. A.: HyGCS: Hydro-Geochemical Classification Suite (v0.5.1). Zenodo.
785 <https://doi.org/10.5281/zenodo.18462921>, 2026.

786

787 Jahan, S. and Strezov, V.: Comparison of pollution indices for the assessment of heavy metals in the sediments of seaports of
788 NSW, Australia, Mar. Pollut. Bull., 128, 295–306, <https://doi.org/10.1016/j.marpolbul.2018.01.036>, 2018.

789

790 Kimball, B. A., Runkel, R. L., Walton-Day, K., and Bencala, K. E.: Assessment of metal loads in watersheds affected by acid
791 mine drainage by using tracer injection and synoptic sampling: Cement Creek, Colorado, USA, Applied Geochemistry, 17,
792 1183–1207, [https://doi.org/10.1016/s0883-2927\(02\)00017-3](https://doi.org/10.1016/s0883-2927(02)00017-3), 2002.

793

794 Knapp, J. L. A., Freyberg, J. von, Studer, B., Kiewiet, L., and Kirchner, J. W.: Concentration–discharge relationships vary
795 among hydrological events, reflecting differences in event characteristics, Hydrol. Earth Syst. Sci., 24, 2561–2576,
796 <https://doi.org/10.5194/hess-24-2561-2020>, 2020.

797

798 Knapp, J. L. A. and Musolff, A.: Concentration–Discharge Relationships Revisited: Overused But Underutilised?, Hydrol.
799 Process., 38, <https://doi.org/10.1002/hyp.15328>, 2024.

800

801 Kuhn, M., and Johnson, K. (1st Ed.): Applied Predictive Modeling, Springer, New York, 600 pp., ISBN 978-1-4614-6849-3,
802 2013.

803

804 Kumar, V., Paul, D., and Kumar, S.: Acid mine drainage from coal mines in the eastern Himalayan sub-region:
805 Hydrogeochemical processes, seasonal variations and insights from hydrogen and oxygen stable isotopes, Environ. Res., 252,
806 119086, <https://doi.org/10.1016/j.envres.2024.119086>, 2024.

807

808 Länderarbeitsgemeinschaft Wasser (LAWA): Arbeitshilfe zur Umsetzung der EG-Wasserrahmenrichtlinie,
809 https://www.lawa.de/documents/arbeitshilfe_30-04-2003_152293505.pdf, 2003.

810

811 Lemenkova, P.: Evaluating the Performance of Palmer Drought Severity Index (PDSI) in Various Vegetation Regions of the
812 Ethiopian Highlands, Acta Biologica Marisiensis, 2021, 14–31, <https://doi.org/10.2478/abmj-2021-0010>, n.d.

813

814 Li, L., Bao, C., Sullivan, P. L., Brantley, S., Shi, Y., and Duffy, C.: Understanding watershed hydrogeochemistry: 2.
815 Synchronized hydrological and geochemical processes drive stream chemostatic behavior, Water Resour. Res., 53, 2346–2367,
816 <https://doi.org/10.1002/2016wr018935>, 2017.

817

818 Li, Q., Ma, L., and Liu, T.: Transformation among precipitation, surface water, groundwater, and mine water in the Hailiutu
819 River Basin under mining activity, Journal of Arid Land, 14, 620–636, <https://doi.org/10.1007/s40333-022-0020-1>, 2022.

820

821 Liu, G., Xue, W., Tao, L., Liu, X., Hou, J., Wilton, M., Gao, D., Wang, A., and Li, R.: Vertical distribution and mobility of
822 heavy metals in agricultural soils along Jishui River affected by mining in Jiangxi Province, China, Clean - Soil, Air, Water,
823 42, 1450–1456, <https://doi.org/10.1002/clen.201300668>, 2014.

824

825 Lloyd, C. E. M., Freer, J. E., Johnes, P. J., and Collins, A. L.: Technical Note: Testing an improved index for analysing storm
826 discharge–concentration hysteresis, Hydrol. Earth Syst. Sci., 20, 625–632, <https://doi.org/10.5194/hess-20-625-2016>, 2016.

827

828 Macklin, M. G., Thomas, C. J., Mudbhakal, A., Brewer, P. A., Hudson-Edwards, K. A., Lewin, J., Scussolini, P., Eilander,
829 D., Lechner, A., Owen, J., Bird, G., Kemp, D., and Mangalaa, K. R.: Impacts of metal mining on river systems: a global
830 assessment, Science, 381, 1345–1350, <https://doi.org/10.1126/science.adg6704>, 2023.

831

832 McClain, M. E., Boyer, E. W., Dent, C. L., Gergel, S. E., Grimm, N. B., Groffman, P. M., Hart, S. C., Harvey, J. W., Johnston,
833 C. A., Mayorga, E., McDowell, W. H., and Pinay, G.: Biogeochemical Hot Spots and Hot Moments at the Interface of
834 Terrestrial and Aquatic Ecosystems, Ecosystems, 6, 301–312, <https://doi.org/10.1007/s10021-003-0161-9>, 2003.

835

836 McDonnell, J. J., Spence, C., Karran, D. J., Meerveld, H. J. van, and Harman, C. J.: Fill-and-Spill: A Process Description of
837 Runoff Generation at the Scale of the Beholder, *Water Resources Research*, 57, <https://doi.org/10.1029/2020wr027514>, 2021.

838

839 McKinney, W.: *Data Structures for Statistical Computing in Python*, in: Proceedings of the 9th Python in Science Conference,
840 edited by van der Walt, S. and Millman, J., 51–56, 2010.

841

842 Merritt, P. and Power, C.: Assessing the long-term evolution of mine water quality in abandoned underground mine workings
843 using first-flush based models, *Science of the Total Environment*, 846, <https://doi.org/10.1016/j.scitotenv.2022.157390>, 2022.

844

845 Milly, P. C. D., Wetherald, R. T., Dunne, K. A., and Delworth, T. L.: Increasing risk of great floods in a changing climate,
846 *Nature*, 415, 514–517, <https://doi.org/10.1038/415514a>, 2002.

847

848 Mischo, U.-P. D.-I. H., Eng, P., Barakos, D.-I. G., Szkliniarz, K., and Kisiel, J.: SITE DESCRIPTION AND DATA OF THE
849 Reiche Zeche Site services, Characteristics and Data, 2021.

850

851 Mugova, E. and Wolkersdorfer, C.: Density stratification and double-diffusive convection in mine pools of flooded
852 underground mines – A review, *Water Research*, 214, <https://doi.org/10.1016/j.watres.2021.118033>, 2022.

853

854 Mugova, E., Molaba, L., and Wolkersdorfer, C.: Understanding the Mechanisms and Implications of the First Flush in Mine
855 Pools: Insights from Field Studies in Europe's Deepest Metal Mine and Analogue Modelling, *Mine Water Environ.*, 43, 73–
856 86, <https://doi.org/10.1007/s10230-024-00969-3>, 2024.

857

858 Munn, S., Aschberger, K., Olsson, H., Pakalin, S., Pellegrini, G., Vegro, S., and Paya Perez, A.: European Union Risk
859 Assessment Report - Zinc Metal. Publications Office of the European Union, Luxembourg, ISBN 978-92-79-17540-4, 2010.

860

861 Musolff, A., Fleckenstein, J. H., Rao, P. S. C., and Jawitz, J. W.: Emergent archetype patterns of coupled hydrologic and
862 biogeochemical responses in catchments, *Geophysical Research Letters*, 44, 4143–4151,
863 <https://doi.org/10.1002/2017gl072630>, 2017.

864

865 Musolff, A., Schmidt, C., Selle, B., and Fleckenstein, J. H.: Catchment controls on solute export, *Adv. Water Resour.*, 86,
866 133–146, <https://doi.org/10.1016/j.advwatres.2015.09.026>, 2015.

867

868 Musolff, A., Zhan, Q., Dupas, R., Minaudo, C., Fleckenstein, J. H., Rode, M., Dehaspe, J., and Rinke, K.: Spatial and Temporal
869 Variability in Concentration-Discharge Relationships at the Event Scale, *Water Resour. Res.*, 57,
870 <https://doi.org/10.1029/2020wr029442>, 2021.

871

872 Palmer, S. M., Evans, C. D., Chapman, P. J., Burden, A., Jones, T. G., Allott, T. E. H., Evans, M. G., Moody, C. S., Worrall,
873 F., and Holden, J.: Sporadic hotspots for physico-chemical retention of aquatic organic carbon: from peatland headwater source
874 to sea, *Aquat. Sci.*, 78, 491–504, <https://doi.org/10.1007/s00027-015-0448-x>, 2016.

875

876 Pandas development team: *pandas-dev/pandas: Pandas*, Zenodo, <https://doi.org/10.5281/zenodo.3509134>, 2020.

877

878 Plotly Technologies Inc.: *Collaborative data science*, Plotly, Montreal, QC, <https://plotly.com>, 2015.

879

880 Pohle, I., Baggaley, N., Palarea-Albaladejo, J., Stutter, M., and Glendell, M.: A Framework for Assessing Concentration-
881 Discharge Catchment Behavior From Low-Frequency Water Quality Data, *Water Resources Research*, 57,
882 <https://doi.org/10.1029/2021wr029692>, 2021.

883

884 Resongles, E., Casiot, C., Freydier, R., Gall, M. L., and Elbaz-Poulichet, F.: Variation of dissolved and particulate metal(lloid)
885 (As, Cd, Pb, Sb, Tl, Zn) concentrations under varying discharge during a Mediterranean flood in a former mining watershed,
886 the Gardon River (France), *Journal of Geochemical Exploration*, 158, <https://doi.org/10.1016/j.gexplo.2015.07.010>, 2015.

887

888 Roberts, M. E., Kim, D., Lu, J., and Hamilton, D. P.: HARP: A suite of parameters to describe the hysteresis of streamflow
889 and water quality constituents, *J. Hydrol.*, 626, 130262, <https://doi.org/10.1016/j.jhydrol.2023.130262>, 2023.

890

891 Rose, L. A., Karwan, D. L., and Godsey, S. E.: Concentration–discharge relationships describe solute and sediment
892 mobilization, reaction, and transport at event and longer timescales, *Hydrological Processes*, 32, 2829–2844,
893 <https://doi.org/10.1002/hyp.13235>, 2018.

894

895 Sächsisches Landesamt für Umwelt, Landwirtschaft und Geologie (LfULG): <https://lfulg.sachsen.de/>, last access: 11 July
896 2025.

897

898 Sanchez, A. A., Haas, K., Jackisch, C., Hedrich, S., and Lau, M. P.: Enrichment of dissolved metal(lloid)s and microbial organic
899 matter during transit of a historic mine drainage system, *Water Res.*, 266, 122336,
900 <https://doi.org/10.1016/j.watres.2024.122336>, 2024.

901

902 Sanchez, A. A., Jackisch, C., Oelschlägel, M., Hedrich, S., and Lau, M. P.: Harmful metal export from abandoned mines
903 controlled by hydrodynamic and biogeochemical drivers. *ACS ES&T Water. Article ASAP*,
904 <https://10.1021/acsestwater.5c00334>, 2025.

905

906 Sanchez, A. A., Lau, M. P., Adam, S. P., Haas, K. J., Hedrich, S., and Jackisch, C.: LegacyMine_HydroGeo: Dataset on
907 geochemical and hydrological dynamics in a historic mine system [Data set]. <https://b2share.eudat.eu.https://doi.org/10.23728/b2share.566z6-gtm46>, 2026.

908

909

910 Schmadel, N. M., Harvey, J. W., Alexander, R. B., Schwarz, G. E., Moore, R. B., Eng, K., Gomez-Velez, J. D., Boyer, E. W.,
911 and Scott, D.: Thresholds of lake and reservoir connectivity in river networks control nitrogen removal, *Nat. Commun.*, 9,
912 2779, <https://doi.org/10.1038/s41467-018-05156-x>, 2018.

913

914 Sergeant, C. J., Sexton, E. K., Moore, J. W., Westwood, A. R., Nagorski, S. A., Ebersole, J. L., Chambers, D. M., O’Neal, S.
915 L., Malison, R. L., Hauer, F. R., Whited, D. C., Weitz, J., Caldwell, J., Capito, M., Connor, M., Frissell, C. A., Knox, G.,
916 Lowery, E. D., Macnair, R., Marlatt, V., McIntyre, J. K., McPhee, M. V., and Skuce, N.: Risks of mining to salmonid-bearing
917 watersheds, *Sci. Adv.*, 8, eabn0929, <https://doi.org/10.1126/sciadv.abn0929>, 2022.

918

919 Shaw, M., Yazbek, L., Singer, D., and Herndon, E.: Seasonal mixing from intermittent flow drives concentration-discharge
920 behaviour in a stream affected by coal mine drainage, *Hydrological Processes*, 34, 3669–3682,
921 <https://doi.org/10.1002/hyp.13822>, 2020.

922

923 Spangenberg, J. E., Dold, B., Vogt, M. L., and Pfeifer, H. R.: Stable hydrogen and oxygen isotope composition of waters from
924 mine tailings in different climatic environments, *Environmental Science and Technology*, 41, 1870–1876,
925 <https://doi.org/10.1021/es061654w>, 2007.

926

927 Speir, S. L., Rose, L. A., Blaszcak, J. R., Kincaid, D. W., Fazekas, H. M., Webster, A. J., Wolford, M. A., Shogren, A. J., and
928 Wymore, A. S.: Catchment concentration–discharge relationships across temporal scales: A review, *Wiley Interdiscip. Rev.:
929 Water*, 11, <https://doi.org/10.1002/wat2.1702>, 2024.

930

931 Sprenger, M., Leistert, H., Gimbel, K., and Weiler, M.: Illuminating hydrological processes at the soil-vegetation-atmosphere
932 interface with water stable isotopes, *Reviews of Geophysics*, 54, 674–704, <https://doi.org/10.1002/2015rg000515>, 2016.

933

934 Turnbull, L., Hütt, M.-T., Ioannides, A. A., Kininmonth, S., Poepll, R., Tockner, K., Bracken, L. J., Keesstra, S., Liu, L.,
935 Masselink, R., and Parsons, A. J.: Connectivity and complex systems: learning from a multi-disciplinary perspective, *Appl.*
936 *Netw. Sci.*, 3, 11, <https://doi.org/10.1007/s41109-018-0067-2>, 2018.

937

938 Tichomirova, M., Heidel, C., Junghans, M., Haubrich, F., and Matschullat, J.: Sulfate and strontium water source identification
939 by O, S and Sr isotopes and their temporal changes (1997–2008) in the region of Freiberg, central-eastern Germany, *Chem.*
940 *Geol.*, 276, 104–118, <https://doi.org/10.1016/j.chemgeo.2010.06.004>, 2010.

941

942 Tomlinson, D. L., Wilson, J. G., Harris, C. R., and Jeffrey, D. W.: Problems in the assessment of heavy-metal levels in estuaries
943 and the formation of a pollution index, *Helgoländer Meeresunters.*, 33, 566–575, <https://doi.org/10.1007/bf02414780>, 1980.

944

945 Vaughan, M. C. H., Bowden, W. B., Shanley, J. B., Vermilyea, A., Sleeper, R., Gold, A. J., Pradhanang, S. M., Inamdar, S.
946 P., Levia, D. F., Andres, A. S., Birgand, F., and Schroth, A. W.: High-frequency dissolved organic carbon and nitrate
947 measurements reveal differences in storm hysteresis and loading in relation to land cover and seasonality, *Water Resources*
948 *Research*, 53, 5345–5363, <https://doi.org/10.1002/2017wr020491>, 2017.

949

950 Vidon, P., Allan, C., Burns, D., Duval, T. P., Gurwick, N., Inamdar, S., Lowrance, R., Okay, J., Scott, D., and Sebestyen, S.:
951 Hot Spots and Hot Moments in Riparian Zones: Potential for Improved Water Quality Management1, *JAWRA J. Am. Water*
952 *Resour. Assoc.*, 46, 278–298, <https://doi.org/10.1111/j.1752-1688.2010.00420.x>, 2010.

953

954 Wells, N., Goddard, S., and Hayes, M. J.: A Self-Calibrating Palmer Drought Severity Index, *J. Clim.*, 17, 2335–2351,
955 [https://doi.org/10.1175/1520-0442\(2004\)017<2335:aspdsi>2.0.co;2](https://doi.org/10.1175/1520-0442(2004)017<2335:aspdsi>2.0.co;2), 2004.

956

957 Wilson, S. R., Hoyle, J., Measures, R., Ciacca, A. D., Morgan, L. K., Banks, E. W., Robb, L., and Wöhling, T.: Conceptualising
958 surface water–groundwater exchange in braided river systems, *Hydrol. Earth Syst. Sci.*, 28, 2721–2743,
959 <https://doi.org/10.5194/hess-28-2721-2024>, 2024.

960

961 Winter, C., Lutz, S. R., Musolff, A., Kumar, R., Weber, M., and Fleckenstein, J. H.: Disentangling the Impact of Catchment
962 Heterogeneity on Nitrate Export Dynamics From Event to Long-Term Time Scales, *Water Resour. Res.*, 57,
963 <https://doi.org/10.1029/2020wr027992>, 2021.

964

965 Zhiteneva, V., Brune, J., Mischo, H., Weyer, J., Simon, A., and Lipson, D.: Reiche Zeche Mine Water Geochemistry, 2016.

966

967 Zuecco, G., Penna, D., Borga, M., and Meerveld, H. J. van: A versatile index to characterize hysteresis between hydrological
968 variables at the runoff event timescale, *Hydrol. Process.*, 30, 1449–1466, <https://doi.org/10.1002/hyp.10681>, 2016.

969